Sede Amministrativa: Università degli Studi di Padova

Dipartimento di *Biologia*

SCUOLA DI DOTTORATO DI RICERCA IN : Bioscienze e Biotecnologie
INDIRIZZO: Biochimica e Biofisica
CICLO XXVI

TITOLO TESI

STRUCTURAL FEATURES OF THE INTRACELLULAR DOMAINS OF THE CYSTIC FIBROSIS TRANSMEMBRANE CONDUCTANCE REGULATOR.

Direttore della Scuola : Ch.mo Prof. Giuseppe Zanotti
Coordinatore d'indirizzo: Ch.mo Prof. Fabio Di Lisa
Supervisore : Ch.mo Prof.sa Maria Catia Sorgato
Ch.mo Dott. Oscar Moran

Dottorando : Lauretta Galeno

A mia madre, alla mia famiglia.

Acknowledgements

This work was supported by the Fondazione Ricerca Fibrosi Cistica (grant #2/2008); Mille bambini a Via Margutta - onlus, Blunotte and Lega Italiana FC - Associazione Toscana Onlus, and by the Italian Cystic Fibrosis Research Foundation (grant #7/2010), with the collaboration of the Delegazione FFC di Cosenza 2, Work in Progress Communication "Sapore di Sale 2010", Gruppo di Sostegno di Monterotondo (RM), Delegazione FFC di Genova, Delegazione FFC "Il Sorriso di Jenny", LIFC Comitato provinciale di Livorno.

I would like to thank Prof. M. Catia Sorgato for the continuous encouragement, and Prof. Oscar Moran for all the teaching I received to grow up as a scientist.

My thanks go also to Elena Galfrè for the crucial help in the biochemical assays, to Carlotta Marasini for the CD spectra analysis, to Prof. Oscar Moran for the SAXS spectra analysis and to every one of the Institute of Biophysics of the CNR, Genova, for their help and support, and for rendering these years enjoyable even when life became “not that easy”.

Contents

Abbreviations

CF	Cystic Fibrosis
CFTR	Cystic Fibrosis Transmenbrane conductance Regulator
NBD	Nucleotide Binding Domain
RD	Regulatory Domain
SAXS	Small Angle X-ray Scattering
PBF	2-Pyrimidin-7,8-BenzoFlavone
CD	Circular Dichroism
PI	Pancreatic Insufficiency
PS	Pancreatic Sufficiency
PTC	Premature Termination Codon
ASL	Airway Surface Liquid
WT	Wild Type
ER	Endoplasmic Reticulum
MSD1	Membrane Spanning Domain 1
Hsp-40	Heat shock protein 40 kD
Hsp-70	Heat shock protein 70 kD
MSD2	Membrane Spanning Domain 2
F	Phenylalanine
PK	pyruvate kinase
PKA	Protein Kinase A
PKC	Protein Kinase C
ATP	Adenosine Triphosphate
TM	Transmembrane
ADP	Adenosine Diphosphate
ENaC	Epithelial Sodium (Na) Channel
PCL	Periciliary Liquid
CaCC	Calcium-activated Chloride Channel
ABC	ATP- Binding-Cassette
RI	Regulatory insertion
RE	Regulatory Extension
YFP	Yellow Fluorescent Protein
VX-770	Ivacaftor
VX-809	Lumacaftor
LB	Luria Broth
IPTG	Isopropyl-β-D-1-Thiogalactopyranoside
EDTA	Ethylenediaminetetraacetic acid
DTT	Dithiothreitol
kDa	Kilodaltons
PBS	Phosphate Buffered Saline
Kd	dissociation constant
ΔF	difference of fluorescence
NADH	Nicotinamide adenine dinucleotide reduced
Km	Michaelis–Menten constant
Vmax	maximum velocity of the reaction

θ	ellipticity
λ	wavelength of X-ray beam
I	scattered intensity
Rg	radius of gyration
R_S	Stoke radius
D_{max}	maximum particle diameter
DAMMIN	Dummy Atom Model Minimization
EOM	Ensemble Optimization Method
NSD	Normalize Spatial Discrepancy

Synopsis

Cystic fibrosis (CF) is the most common human genetic disease, occurring prevalently in the Caucasian population at a rate of 1 to 2500 newborns. It is an autosomal recessive disease caused by mutations in the cystic fibrosis trans-membrane conductance regulator (CFTR) gene, which encodes a chloride channel expressed mainly in epithelial cells, but which is also involved in the bicarbonate–chloride exchange. The most common CF symptoms include progressive lung disease and chronic problems of the digestive apparatus (Riordan et al., 1989), whose degree of severity depends on other genetic and/or environmental factors. CF pathogenesis is characterised by the build-up of thick, sticky mucus in multiple mucin-producing organs, such as lungs, sinuses, intestine, pancreas and reproductive organs. For this reason, CF is also denominated mucoviscidosis, implying that mucins - polymeric, gel-forming O-linked glycoproteins responsible for the viscoelastic properties of the mucus - play a critical role in the disease (Kreda et al., 2012).

The aim of the present Ph. D. work was to investigate the structural features of two CFTR domains: the nucleotide binding domains (NBDs) - responsible for the gating mechanisms of the channel, and which have been proposed to serve as drug targets - and the regulatory domain (RD), directly involved in the activation of the channel. Knowledge of these aspects could likely improve understanding of the aberrant functionality of defective CFTR, and also help designing therapeutic strategies to either correct the defective protein *in situ*, and/or to potentiate its physiologic channel activity.

The present thesis refers essentially to the four published papers containing most of the results obtained during the 3 year-doctorate course. The first one reports on some biochemical and structural features of NBDs, which were investigated using biochemical assays and measures of small angle x ray scattering (SAXS), while the second paper dealt with the interaction of NBDs

with a potentiator (2-pyrimidin-7,8-benzoflavone, PBF) of CFTR activity. Instead, the third and the fourth papers considered RD under non-phosphorylated and phosphorylated conditions, and the influence of phosphorylation on the conformation of the domain as followed by circular dichroism (CD) and SAXS experiments.

Briefly, the obtained results allowed us to draw the following principal conclusions.

NBDs When in an equimolar mixture and in the presence of ATP, NBDs form a dimer, whose conformation can be significantly changed by PBF. In addition, data could be exploited to reconstruct the *ab-initio* model of NBDs both as dimer (with or without PBF) and as isolated monomers.

RD In this case, obtained results on biochemical, structural and thermodynamic RD aspects allowed us to reconstructing a low-resolution, 3-D model of the native and phosphorylated protein, and to underline how phosphorylation induces the conformational change of the domain and the decreasing of RD stability.

I - Introduction

1- CFTR: amino acid composition and mutations

The gene that encodes CFTR is on the long arm of human chromosome 7, region q31-q32. The gene has recently been identified and shown to be approximately 250 kb in size, comprising 27 exons (Zielenski et al., 1991). CFTR orthologs have also been identified in all mammals. CFTR is identified by its primary sequence P13569 (CFTR_HUMAN) (UniProtKB/Swiss-Prot). After the splicing process, a 6.5 kb mRNA that includes all exons is produced and translated to generate functional CFTR (Fanen et al., 2014). More than 1,500 CFTR mutations have been identified (http://www.sickkids.ca/), although for only a small number the functional importance is known.

1.1 - Classification of CFTR mutations based on CF clinical consequences

In 2007, during the Consensus Conference organized by the European Cystic Fibrosis Society, the European Society of Human Genetics and the Euro Gentest Network of Excellence established to classily CFTR mutations into four (A-D) groups based on their clinical consequences (Castellani et al., 2008; Fanen et al., 2014). However, in order to appreciate this classification, it is firstly necessary to briefly expose CF main phenotypes.

The majority of CF patients suffer from “classic” CF, with either an exocrine pancreatic insufficiency (PI) or pancreatic sufficiency (PS), and show a sweat chloride concentration of >60 mmol/L. Indeed the disease can have a severe course, with rapid progression of symptoms, or a milder course with very little deterioration of organs functionality over time. Classic CF generally evolves to progressive respiratory problems, and from a genetic standpoint it is characterized by one established CF-causing mutation on each CFTR allele. In contrast, non-classic CF (e.g. chronic pancreatitis, allergic broncho pulmonary Aspergillosis and sclerosing cholangitis), is typical of individuals with at least one of the previously described CF symptoms but with a normal (<30

mmol/L), or borderline (30-60 mmol/L), sweat chloride level. It is diagnosed by detection of a mutation on each CFTR allele, or by direct quantification of CFTR dysfunction by the Nasal Potential Difference Test (Boyle, 2003; Rosenstein, 2003).

Thus, two types of classification of CFTR mutations have been produced.

Classification based on clinical aspects

- Group A: it comprises 23 mutations that cause classic CF, which include missense, stop, splicing and frame-shift mutations, e.g., F508del.
- Group B: it includes mutations that cause non-classic CF (associated to CFTR-related disorders), e.g., TG13-T5a, R117H-T5a, D1152Ha.
- Group C: it comprises mutations with as yet unknown clinical consequences, e.g., TG11-T5b, R117H-T7b, R75Qb.
- Group D: it consists of mostly missense mutations with an as yet undefined, or uncertain, clinical relevance.

Only a few of the hundreds to date-identified CFTR mutations result in classic CF, and within a given ethnic group, specific mutations may be more frequent than others. As mentioned, F508del is one severe classic mutation, which accounts for approximately 70% of worldwide CF mutants; most CF patients are Caucasian but other ethnicities are also affected (Lucotte et al., 1995).

Classification based on CFTR functional consequences

In light of the above-mentioned (see "synopsis) physiological aspects of CFTR, a classification (into five major classes) of CFTR mutations was established according to their consequences on CFTR processing or function (Welsh and Smith, 1993).

- Class I mutations: those which interfere with CFTR synthesis, and which result in the total, or partial, loss of production of functional CFTR. Such mutations may arise from: (1), a nucleotide substitution introducing an in-frame premature termination codon (PTC) - UAA, UAG or UGA -; (2), frame-shifting insertions or deletions; (3), mutations at the invariant dinucleotide splice junctions, or introduction of a PTC, resulting in the skipping of an out-of-frame exon; (4), a gene rearrangement altering the exon sequence.
- Class II mutations: those which affect CFTR maturation in such a way that not all CFTR are properly folded, or transported to the cell surface. Defective CFTR then undergoes the proteasomal degradative process. This class of mutations include the most prevalent CF mutation, F508del (according to the Cystic Fibrosis Foundation Patient Registry (Cystic Fibrosis Foundation. Patient registry annual data report 2010) (MacDonald et al., 2007)).
- Class III mutations: those which alter the gating of the CFTR channel; they affect only a small (2-3%) percentage of patients. Thus, CFTR is able to reach the cell membrane but the channel does not open properly and Cl^- transport cannot take place. This class of mutations includes G551D (the most common), S492F, V520F, R553G, R560T and R560S (Rogan et al., 2011; O'Sullivan et al., 2009).
- Class IV mutations: those which provoke the narrowing of the CFTR channel and affect a small percentage (2%) of patients. Mutation of this class are: A455E, R117C, D1152H, L227R, R334T, R117H (Rogan et al., 2011; O'Sullivan et al., 2009).

- Class V mutations: those which reduce the amount of CFTR that functions normally. They are due to splicing defects that result in improper mRNA processing. Therefore, a reduced number of CFTR reaches the surface in which, however, they are capable to transport chloride effectively. In some cases, CF patients may be asymptomatic, as in the case of: 3849+10kb C→T;1811+1-6kb A→G; IVS8-5T; 2789+5G→A (Rogan et al., 2011; O'Sullivan et al., 2009).

A (VI) class of mutations that decreases the stability of CFTR at the plasma membrane was proposed. However, due to its still poor characterization (Haardt et al., 1999), these mutations are now combined with class V (Welsh et al., 2001; Fanen et al., 2014).

There is a demonstrated relationship between the CFTR mutation functional class on both alleles and pulmonary functionality in adult CF patients. Patients with a CFTR mutation belonging to class I or II show significantly lower baseline and current spirometric values, greater loss of pulmonary function during follow up, higher risk of developing moderate to severe pulmonary disease, and a lower rate of survival (due to end-stage lung disease) than patients with (at least) one CFTR mutation of class III-V on one allele. Thus, the genotype, based on functional class mutation on the two alleles, seems one of the most decisive factors for pulmonary damage severity and survival (O'Sullivan et al., 2009).

Table 1 and Figure 1 summarize some aspects caused by the different classes of CFTR mutations (O'Sullivan et al., 2009).

Mutation belonging to	Fallout on CFTR	Presence of functional CFTR on the plasma membrane.
Class I	Total or partial loss of CFTR production	No
Class II	CFTR trafficking defects with subsequent protein degradation	No/substantially reduced
Class III	Defective channel regulation	yes
Class IV	Reduced chloride transport	Yes
Class V	Splicing defects with reduced production of normal CFTR	Yes

Table1 Classification of CFTR mutations and their consequences on the activity or amount of CFTR at the plasma membrane.

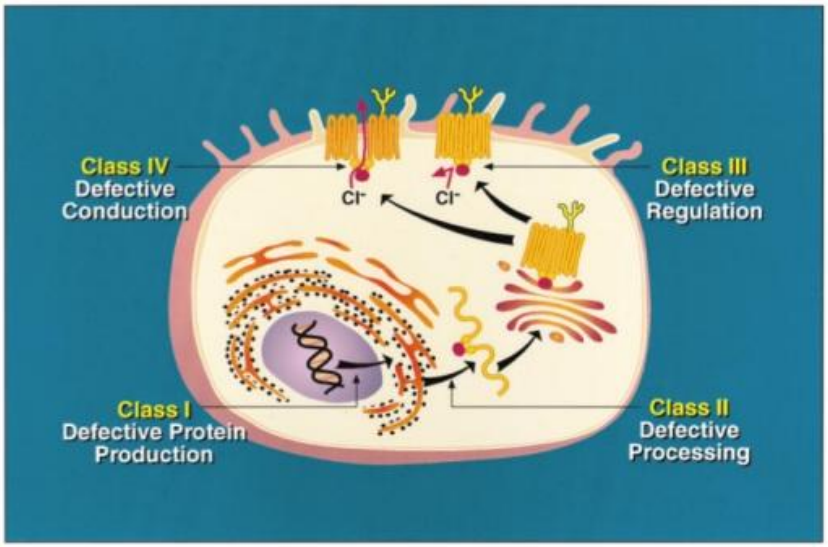

Fig. 1 Mechanisms by which CF-associated mutations cause altered processing and/or function of CFTR (Welsh and Ramse, 1998).

2 - Cystic Fibrosis: clinical aspects

Before discussing CF clinical aspects, it is good to underline that CF ample phenotypic variability has strongly suggested not only to implicate the occurring CFTR mutation, but that other factors, ranging from gene modifiers to environmental (lifestyle, drugs etc.) factors, are also involved (De Boeck et al., 2006).

CF affects several organs that show different types of abnormal mucus secretion or metabolism (Quinton, 1999). The CF phenotype is typically characterized by complex, multi-organ involvement, including pancreatic exocrine function, pulmonary disease, sweat ion imbalance, and, in males, infertility due to obstructive azoospermia. Clinical consequences range therefore from severe (lungs, pancreas, male reproductive tract) to mild (intestine) to asymptomatic (sweat glands) symptoms, depending on the unique biochemical, cellular and physiological profiles of duct-lining epithelia of the affected organ. Organ features, such as high protein load, slow secretion rate, and long, tortuous ductal passages seem to be predisposing factors for the development of the damage. An additional overall complexity of CF is the variability of the clinical manifestations pertaining to a given organ, their degree of severity and the outcome of the disease. In any case, it has been observed a relatively low variability in the case of sweat gland and male infertility (due to bilateral absence of the vas deferens), a higher variability for pancreatic functions, and a very high variability for the respiratory system (Zielenski, 2000).

Another aspect to be considered in CF is that, whereas a specific CFTR genotype can predict with high precision the involvement of the pancreas, and/or of the male genital tract, the same feature cannot anticipate other clinical phenotypes (e.g., pulmonary disease). Thus, in addition to CFTR mutations, it has been recognized that factors that determine the overall clinical outcomes fall into the environment or genetic category. The former plays a most important role in modulating

pulmonary disease: e.g., inhalation of pollutants or infectious pathogens; active but also passive smoking, which may significantly modify the pulmonary phenotype in patients with otherwise identical genotype (Campbell et al., 1992).

2.1 - Gastrointestinal tract.

Among gastrointestinal manifestations, the exocrine pancreas is most profoundly and commonly affected in CF, PI affecting 85% of CF patients. In the remaining patients, although the exocrine pancreas is not totally normal, nonetheless it functions sufficiently well so as to exclude the need of enzyme supplementation with meals. PI is closely associated with class I-III mutations, although other genetic aspects and environment factors render weak the genotype-phenotype relationship, especially with regard to lung disease (Drumm et al., 2005). Analysis of certain CFTR mutations in patients with PI and PS phenotypes revealed two (severe and mild) categories of mutations: a severe one confers PI only if paired with another severe mutation; a mild mutation sustains pancreatic function in a dominant fashion (PS), even if the second mutation is severe. Thus mild mutations, belonging to class V, affect only minor features of the CFTR channel activity, and likely provide sufficient amount of functional CFTR that can compensate for the lack of active CFTR provoked by severe mutations belonging to class I-V (Zielenski, 2000).

2.2 - Sweat glands.

Its involvement in CF was closely investigated in patients with different CFTR mutations, by measuring their sweat chloride concentration. These studies showed that certain mild mutations (R117H; A455E; 3849+10kb C $\rightarrow$ T) from class IV or V tend to associate with significantly lower Cl^- sweat levels than severe mutations (ΔF508; 621+1G $\rightarrow$ T; G542X; R553X, etc.). Based on this type of observation, the U.S CF Foundation has approved the use of the Wescor Macroduct Sweat to allow identifying putative CF-affected individuals.

2.3 - Male reproductive tract.

A through mutation screening of patients with congenital bilateral absence of the vas deferens revealed a different spectrum of mutations compared with other CF patients. Typically, the genotype consisted of at least one very mild mutation (predominantly missense or splice variant) uncommon for CF patients, belonging to classes IV or V, producing variable amounts of functional CFTR.

2.4 - Respiratory apparatus.

This system has received the highest attention because lung disease is the main cause of morbidity and mortality in CF patients, and is most evasive in terms of treatment. Lung disease is a primary target for developing therapies against CF, and considerable research effort has been devoted to understanding disease pathogenesis in airways. As mentioned, there is ample variation in the severity of pulmonary disease also in CF patients with the same genotype, probably due to other endogenous, or exogenous, factors. Thus, to date, the complex pathology and multi-stage natural history of lung disease appear the most challenging CF aspects in need of full definition and understanding (Zielenski, 2000). The lung phenotype manifests as failure of airways innate defense against inhaled bacteria, which produce chronic infection in the airways lumen and, ultimately, airway obstruction, bronchiectasis and death (Boucher, 2007).

Several assumptions have been made to connect CFTR mutations to the failure of lung defenses through CFTR ion transport function. The periciliary layer (that extends from the cell surface to the height of the extended cilium) and the mucus layer (which is positioned atop the cilia) cooperate to assure the effective clearance of particles deposited on airway surfaces. The two layers together form the so-called airway surface liquid (ASL). The mucus layer must bind and entrap virtually all deposited particles. Its viscoelastic properties and the beating of cilia induce mucus transport (Randell et al., 2006), and also provide a lubricant activity that prevents adhesion of the mucus

layer to the cell surface (Raviv et al., 2003). The mucus layer is composed of extremely long, highly glycosylated polymer, known as mucins. A combination of mucins MUC5AC and MUC5B secreted by goblet cells and submucosal glands, respectively, constitute this gel layer (Rose and Voynow, 2006). Hydration of the mucus is the dominant variable governing mucus clearance. Individuals with CF, who exhibit a phenotype thought to reflect ASL volume depletion, develop more rapid and severe airway infection and destruction. Inadequate hydration causes mucus adhesion to epithelial surfaces, resulting in obstruction and inflammation, and serving as a nidus for infections, as they occur in CF (Matsui et al., 1998).

3 - CFTR (patho-) physiology

CFTR is a regulated Cl^- channel located to the apical membrane of epithelia. Immunological detection of CFTR has revealed that it is abundant in these cells, including those lining the sweat ducts, small pancreatic ducts, intestinal crypts, lung, and the kidney tubules, consistent with a function in the vectorial ion movements across the epithelium. Several reports have indicated that CFTR is also expressed in the heart and in the central nervous system, but its functional relevance in these tissues has not yet been elucidated (Moran and Zegarra-Moran, 2008).

It has been established that synthesis of the whole CFTR takes ~9 min, and that this applies to both wild-type (WT) and mutant F508del-CFTR. CFTR folding is a complex and hierarchical process taking place in multiple cellular compartments along the secretory pathway and involving several folding machineries. CFTR folds in a modular manner, domain after domain, with the simultaneous insertion of the transmembrane segments into the ER membrane (Fig. 2).

Positioning of the transmembrane MSD1 into the ER membrane represents the first step in CFTR folding, while NBD1 is bound transiently by two molecular chaperones belonging to the Hsp-40 and Hsp-70 family, respectively, to promote NBD1 folding and stabilization during the time required for the synthesis of the RD. The RD interacts with the N-terminal half of CFTR, leading to reduction of Hsp-40 binding. MSD2 is then synthesized, integrated into the ER membrane and this event appears to stabilize NBD1-RD interactions which lead to the release of most of the Hsp-40 from CFTR. Finally, NBD2 is synthesized.

The co-translational folding of each WT-CFTR domain uses substantial amounts of energy. However, it is moderate if compared with the much higher energy needed to fold F508del-CFTR. These facts could explain the limited folding efficiency of WT-CFTR and the large folding inefficiency of F508del-CFTR (Fig. 2) (Pranke and Sermet-Gaudelus, 2014).

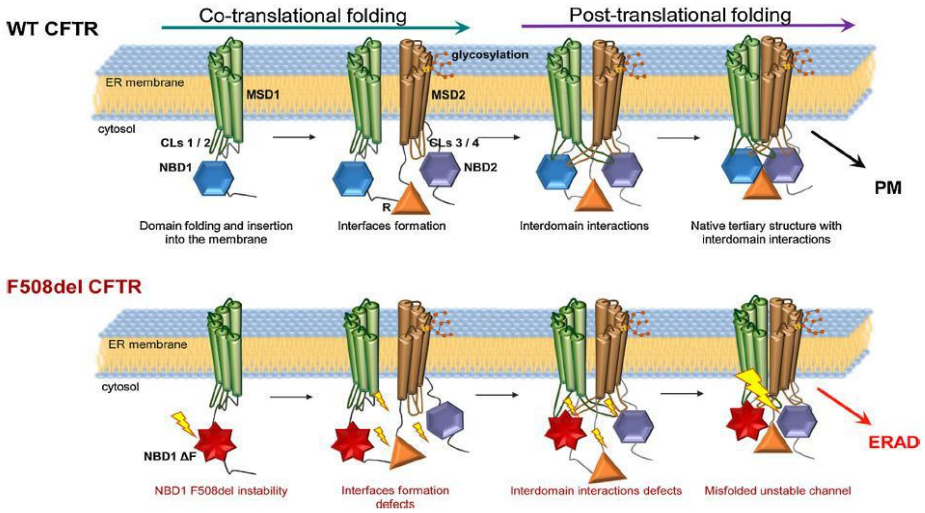

Fig. 2 CFTR folding and domain assembly. CFTR folding and insertion into the membrane starts co-translationally during synthesis of the individual domains, and continues by formation of interfaces and interactions between domains. Correctly folded WT-CFTR with native quaternary structure is then trafficked to the plasma membrane (PM) through the secretory pathway. In contrast, F508del-CFTR folding is strongly affected by the destabilized NBD1 domain, by defects of interface formation and failure of interdomain interactions. Finally, misfolded and unstable F508del-CFTR is rapidly degraded by the ER associated proteasome. MSD1/MSD2 - membrane spanning domain1/2; NBD1/NBD2 - nucleotide binding domain 1, 2; R - regulatory domain; CLs cytoplasmic loops; PM - plasma membrane; ERAD - endoplasmic reticulum-associated degradation (Pranke and Sermet-Gaudelus, 2014).

Because of its dominant contribution to CF, much attention has been focused on the impact of F508del on CFTR folding and assembly. Replacement of the phenylalanine (F), normally present at position 508, by one other amino acids revealed that the presence of many other residues was compatible with substantial folding of the isolated NBD1 domain and the full-length protein (Riordan, 2008). It was also observed that the requirements for maturation of the full-length CFTR were somewhat more stringent with charged, or large hydrophobic, residues than with F, suggesting that the side chain may contribute to inter-domain interactions. Even if the variants that mature show some channel activity, F aromatic side chain apparently plays a specific role in the CFTR channel gating mechanism: variants with either F508S or F508R substitutions lead to only a local surface perturbation around the 508 position, making more realistic the idea that the main impact of the mutation may be the disruption of a crucial interaction between this surface small patch of NBD1 and another part of the molecule (Riordan, 2008).

CFTR is activated by phosphorylation at RD multiple sites by protein kinase A (PKA), and probably also by protein kinase C (PKC). Because phosphorylation by PKA is mandatory for the channel activity, CFTR is also defined as a "cAMP-activated channel". Phosphorylated CFTR channels are then regulated by ATP. The most accepted model for CFTR gating proposes that binding of ATP promotes the dimerization of the NBDs, leading to a conformational change at the level of the TM domains that in turn leads to the channel opening (Fig. 3). The hydrolysis of ATP by the enzymatic activity of NBDs terminates the activity cycle, releasing ADP (Fig. 3), but the energy liberated by ATP hydrolysis is not used to transport chloride. Indeed, once phosphorylated, the channel can be opened also by non-hydrolysable ATP analogues (Aleksandrov et al., 2001).

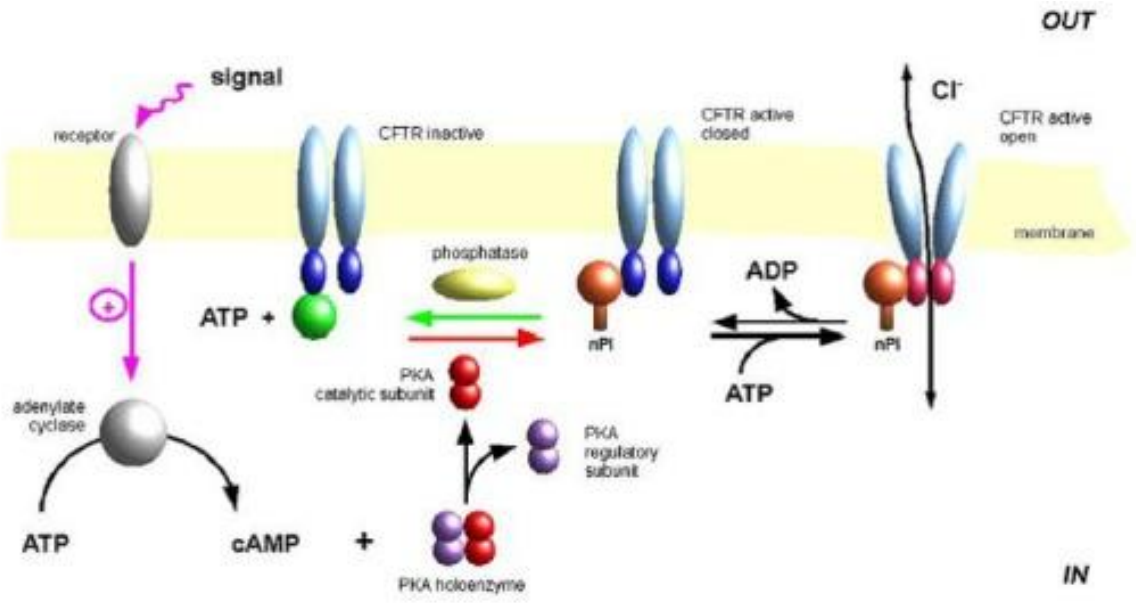

Fig. 3 The functional cycle of CFTR. Protein kinase A (PKA) catalyzes the phosphorylation of the RD domain of CFTR, promoting a conformational transition that leads to active CFTR. The binding of ATP to NBDs induces a second conformational change that gates the channel to the open, Cl^- permeable, conformation. Specifically, the gating cycle of NBDs initiates with the successive binding of two ATP molecules, which induces the dimerization of the domains, by a quasi-irreversible transition, allowing the channel to acquire the open state. By hydrolyzing one ATP, NBDs destabilizes NBD1-NBD2 interactions, which cause the closure of the channel (Moran, 2010; Moran and Zegarra-Moran, 2008).

CFTR activity also serves to maintaining the mucus hydration normal, which is related to its double role as Cl^- channel and as an inhibitor of Na^+ channel (ENaC) (Boucher, 1999) (Fig. 4).

CFTR plays an important role in HCO_3^- secretion because it is permeant to the anion and because it probably stimulates the Cl^-/ HCO_3^- exchange. The most obvious manifestation of the loss of this function is an impaired pancreatic HCO_3^- secretion, but also a reduced pH in the epithelial surface liquid of other tissues. Failure to alkalinize the fluid into which Cl^-/HCO_3^- are secreted is probably

key to preventing the normal processing of mucins and to contributing to their hyper-viscosity (Riordan, 2008).

Although the exact mechanism leading to CF is still a question of debate, undoubtedly the disease is associated with a strong reduction/absence of Cl^- transport across the apical membrane of the epithelium, in such way that the most severe loss of CFTR function is correlated with the most severe CF forms (Moran and Zegarra-Moran, 2008).

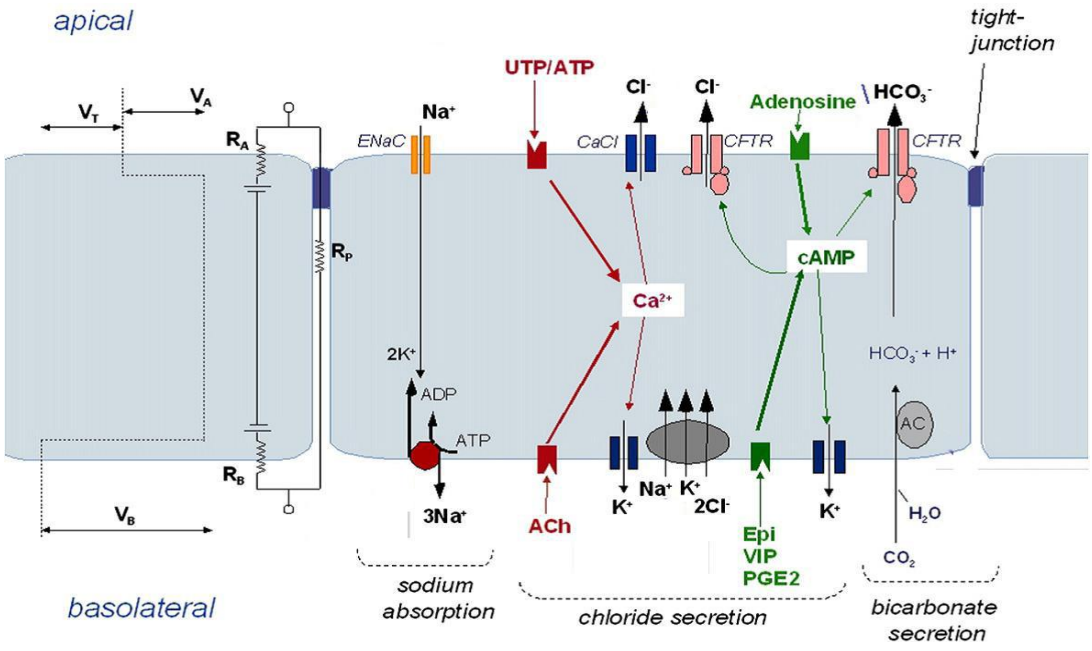

Fig. 4 Schematic representation of epithelial Na^+ and Cl^- transport systems. Na^+ enters the cell from the apical side of the epithelium through the epithelial Na^+ channel (ENaC) and leaves the cell mainly through the Na^+/K^+-ATPase. Cl^- instead enters the cell from the basolateral side through the Na^+-K^+-Cl^- cotransporter (NKCC-co-transporter) and leaves the cell at the apical side either through CFTR or through a Ca^{2+}-dependent channel (CaCl). Thus, Cl^- secretion has been divided into a Ca^{2+}-activated system (in red) and a cAMP-dependent system (in green). An increase of the intracellular Ca^{2+} concentration can be triggered by agonists acting on apical, or basolateral, membrane receptors, such as P2Y receptor activated by UTP or ATP, or the muscarinic receptors activated by acetylcholine (ACh) (Moran and Zegarra-Moran, 2008).

Two different hypothesis have been advanced to describe ASL physiology in normal lungs and dysfunction(s) consequent to CFTR mutations. One is based on the "isosmotic volume hypothesis," and emphasizes the importance of the volume, i.e., height, of the liquid lining the airway surfaces (Boucher, 1994; Boucher, 1999). This hypothesis claims that airway epithelia regulate the height of the liquid surrounding cilia, the periciliary liquid (PCL), to facilitate efficient transduction of energy from the beating cilia to the mucus layer. It thus predicts that, in CF, the accelerated rate of transepithelial Na^+ absorption increases isosmotic volume absorption (Fig. 5), which depletes PCL, and impacts the mucus on airway surfaces that then serves as nidus for chronic infection (Matsui et al., 2000).

Airway epithelia tonically absorb Na^+ through a trans-cellular route, mediated at the apical membrane by the epithelial ENaC and at the basolateral membrane by Na^+-K^+-ATPase. Passive anion flow, which probably reflects the movement of both Cl^- and HCO_3^-, can occur in part transcellularly but the major part occurs through the paracellular path (Fig. 6).

Because the epithelium is water permeable, ion transport is isosmotic, leaving ASL nearly isotonic under basal conditions. The model predicts that the epithelium must finely tune PCL height for efficient mucus transport, suggesting that there are sensors that control the rate of Na^+ transport and, under certain conditions, initiate Cl^- secretion to optimize ASL height/volume. Thus CFTR seems to have functions both as a Cl^- channel and as an ENaC regulator (Boucher, 1999).

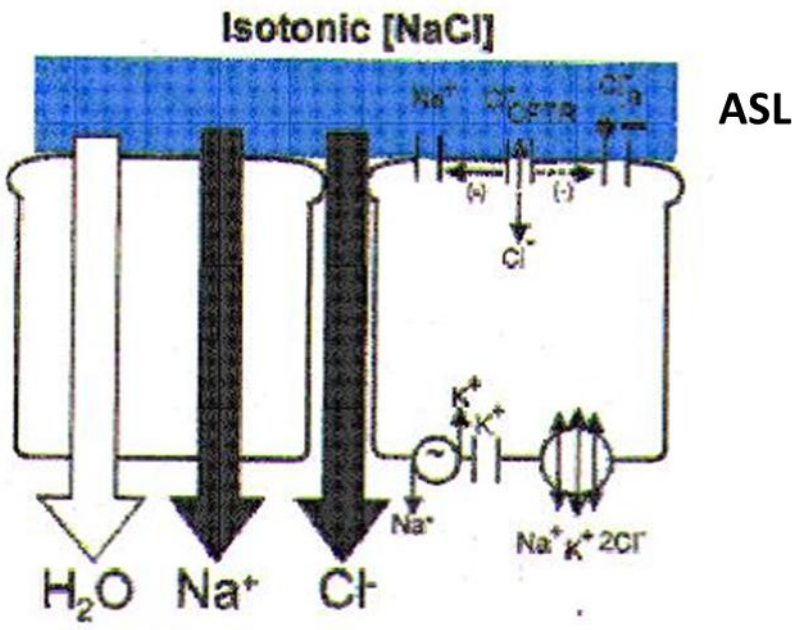

Fig. 5 Model of airway epithelial cells mediating isotonic volume transport. The basolateral Na^+-K^+-ATPase generates the driving force for Na^+ entry across the apical membrane, which is mediated by ENaCs. Both functions of CFTR, as a Cl^- channel (Cl^- CFTR) and as regulator of ENaC, and the alternative (Ca^{2+} -activated) Cl^-channel, are depicted on the apical membrane. Active Na^+ absorption is transcellular, whereas anion flow is, in part, transcellular and, in a larger part, paracellular. The epithelium is quite permeable to water, permitting isosmotic volume transport. Hence, the ASL is designated as isotonic [NaCl] (depicted in dark blue) (Boucher, 1999).

The other hypothesis describes normal airway surfaces as systems that absorb salt, but not water, from airway surfaces to generate a hyposmotic (low salt) ASL, which is required for the activity of salt-sensitive antimicrobial factors against inhaled bacteria. Thus, normal epithelium lowers the ASL Na^+ and Cl^- concentrations to a [NaCl] value of 50 mM, or less, to promote the activity of antimicrobial defensin-like molecules. According to this theory, at the organ level there would be no major role for mucus in lung defense (Boucher, 1999). Inability to absorb Cl^-, through a Cl^- "impermeable" airway epithelial cell as in CF, renders the airway surface liquids isosmotic (Zabner et al., 1998) or hyperosmotic (Gilljam et al., 1989), effectively inhibiting the activity of antimicrobial factors and leading to chronic infection. (Matsui et al., 2000).

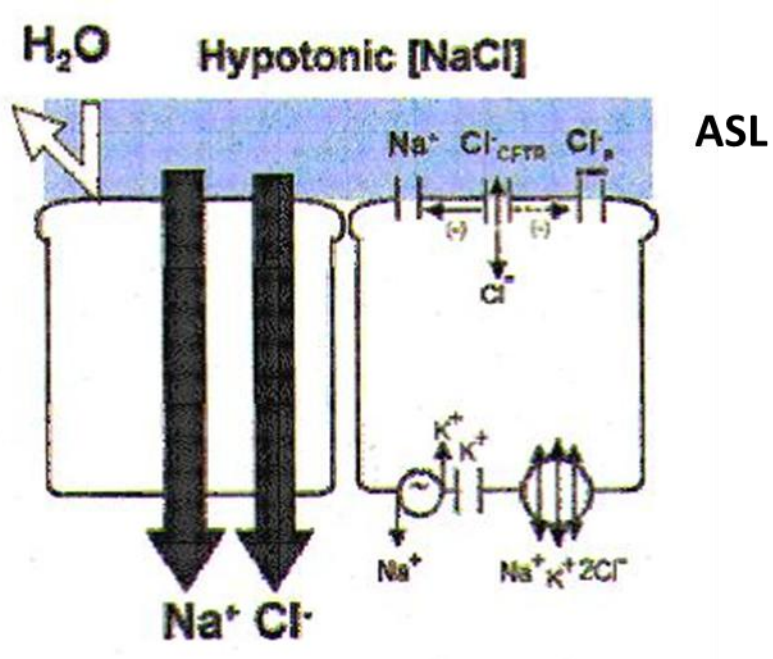

Fig. 6 Physiology of hypotonic airway surface liquid: cell model postulated to explain the production of hypotonic ASL (the 'sweat ductal model'). The key elements are the trans-cellular absorption of Na^+ (via ENaC) and Cl^- (via CFTR) and epithelial water impermeability (depicted as 'deflected' arrow) (Boucher, 1999).

Two signaling pathways seem to be involved in regulating the airway surface liquid volume. One is due to ATP released into the luminal compartment, which then interacts with luminal P2Y2 whose signal inhibits ENaC and activates both CFTR and the calcium-activated chloride channel (Stutts et al., 1995). The other one is also due to ATP, although in this case it starts after ATP degradation to adenosine by surface ectoenzymes. Adenosine interacts with A2b receptors that trigger activation of CFTR (and CFTR-promoted ENaC inhibition) through a cAMP-dependent mechanism (Stutts et al., 1995).

It follows that, in CF airways epithelia, CFTR is not activated, and ENaC is not inhibited, while the consequent lower volume of ASL favors the chronic inflammation of the airway epithelia by allowing colonization by *Pseudomonas* bacteria. Indeed, while bacteria deposited on a normally hydrated mucus gel (2% solid) can 'swim' through the gel and remain in a planktonic state within it,

after salt and water depletion the mucin-dependent meshwork of the CF mucus gel becomes sufficiently ‘tight’ (size of <100 nm) to hamper the mobility of *Pseudomonas* that replicate at the site of deposition faster than their capacity to migrate from it. In addition, lactoferrin and lysozyme that act as antimicrobial agents, or neutrophils, are unable to reach the airway lumen because of the too high concentration of mucus, and the cilia cannot beat normally. Interestingly, although failure of CF lungs to clear infectious microorganisms is generally attributed to impaired mucociliary clearance, it has also been proposed that CFTR itself may serve as a receptor for *Pseudomonas aeruginosa*. In this case, binding of the microbe to CFTR is required for its internalization, which stimulates secretions of the cytokine necessary for clearance (Riordan, 2008).

4 - CFTR structure

CFTR, a member of the ATP-Binding-Cassette (ABC) family, is composed of 1,480 amino acids in the mature form, and forms five domains (Fig. 7). One is the membrane spanning domain (MSD1) (with 6 transmembrane segments), followed by an intracellular nucleotide binding domain (NBD1). This motif is repeated twice, with NBD1 linked to the second MSD2 by a regulatory domain (RD), located to the intracellular compartment, which contains a considerable number of putative phosphorylation sites.

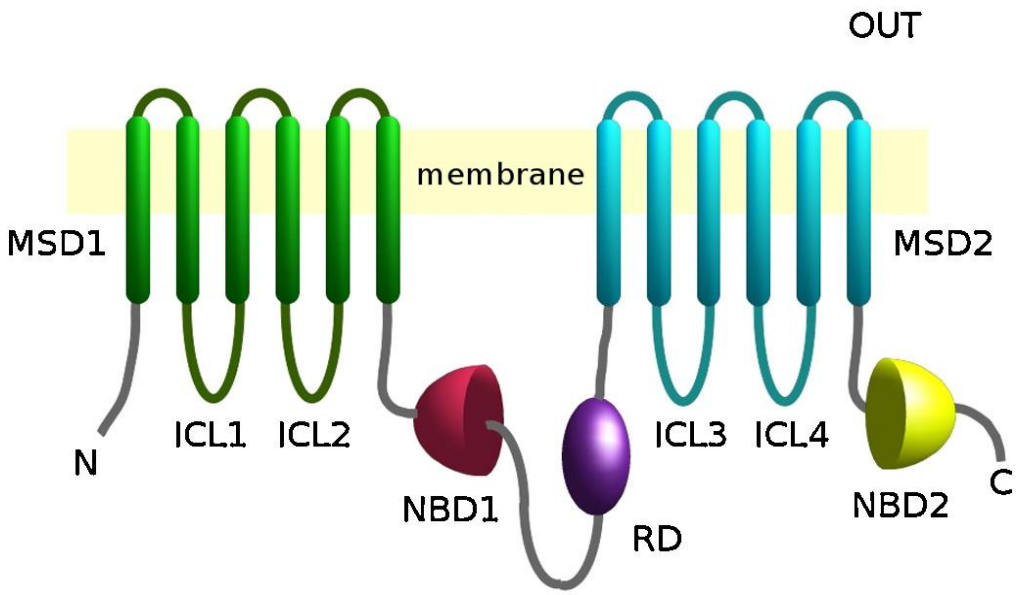

Fig. 7 CFTR structure: MSD1 and MSD2 are the membrane spanning domains; NBD1 and NBD2 are the nucleotide binding domains; RD is the regulatory domain; ICL1 to ICL4 are the intracellular loops 1-4 (from Moran, 2014).

High-resolution structures of eukaryotic ABC transporters have not been determined yet, primarily because of limitations in generating homogeneous mono-disperse preparations of sufficient quality and quantity for large-scale crystallization trials (Riordan, 2008).

Sufficient amounts of CFTR have been purified from mammalian cell expression systems to generate two-dimensional crystalline arrays as well as single particles, allowing to obtain low-resolution 3D structural information (Fig. 8) (Rosenberg et al., 2004).

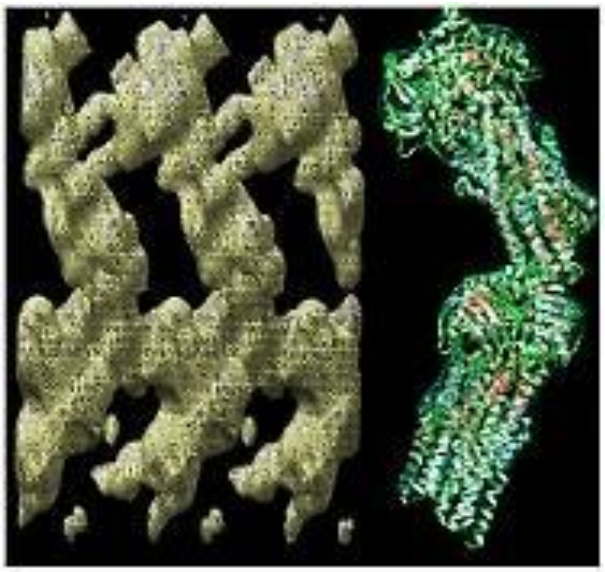

Fig. 8 Electron microscopy map of a bidimensional CFTR crystal. The CFTR map at the left was calculated at a resolution of 18 Å, allowing the molecular envelope of the two CFTR molecules in each unit cell to be clearly seen. Three adjacent unit cells and six CFTR molecules are displayed. The interpretation of the packing in one unit cell is shown at the right (from Rosenberg et al., 2011).

A high resolution structure has been obtained for mouse NBD1 (mNBD1) recombinantly expressed in bacteria. It has the same basic fold as that of the NBDs of many bacterial ABC proteins determined earlier, as well as of several ABC proteins determined earlier. The mNBD1 domain has a core tertiary structure similar to NBDs from other ABC transporters, but this core is modified with major additions and deletions. Figure 10 shows a topology diagram of mNBD1, indicating through color coding the subdomains and those regions of mNBD1 that show significant differences from other ABC structure. Secondary structural elements in common with most known ABC structures are given conventional designations (S1, S2, S3, H1, etc.) and additional elements found in mNBD1 are denoted with lowercase letters (H1b, H1c, S6b, etc.) (Lewis et al., 2004) (Fig. 10).

Most significantly the Phe508 residue occupies a position on the surface of the wild-type domain, and its absence has only minor effects on the domain structure (Lewis et al., 2005), as indicated in Figure 9 (Riordan, 2008).

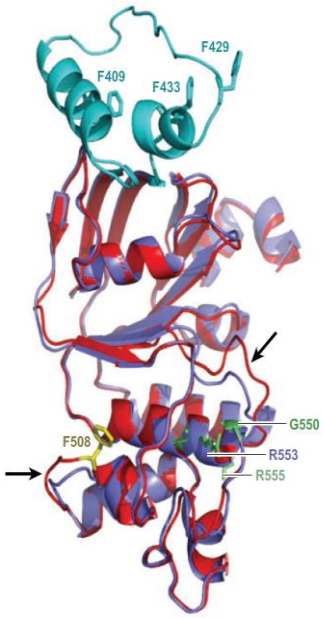

Fig. 9 Structures pertaining to human WT- and F508del-NBD1. Their alignment structures of CFTR are indicated in red for the WT (Protein Data Bank id: 2BBO) and in purple for F508del (Protein Data Bank id: 1XMJ) (http://pymol.sourceforge.net/). The regulatory domain, which is missing from the NBD1 crystal structure, is inserted from a loop database search (SYBL,Tripos Inc., CA). That loop contains (cyan) two α-helixes in good agreement with hydrophobic patch analysis of this region (Riordan, 2008).

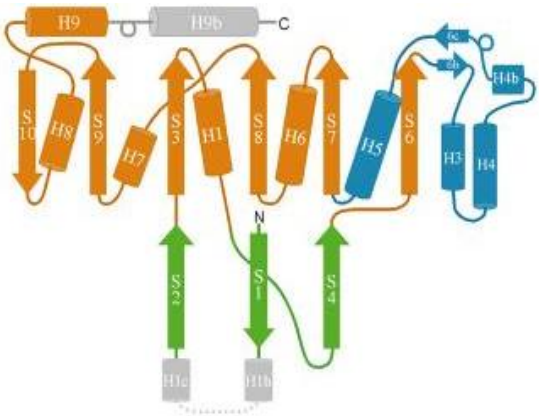

Fig. 10 Topology diagram of mNBD1. The F1-type ATP-binding core subdomain is shown in gold, the ABC α-subdomain in cyan, and the ABC β-subdomain in green. Regions of mNBD1 that are different from other ABC structures are shown in gray.

mNBD1 contains a loop-forming 35-residue stretch with serine residues (named the regulatory insertion, RI) (Lewis et al., 2004). The phosphorylation of these serines imparts order to the structure of the entire RI (Fig. 11); sites of phosphorylation in mNBD1-P are all located on the S1–S2 insertion and on the H9b extension (Fig. 10), and these clashing segments might possibly be displaced when phosphorylated to take up favorable interactions with other parts of CFTR, thereby promoting and maintaining NBD association. This hypothesis is consistent with data from R-domain deletions, which release CFTR gating inhibitions upon phosphorylation (Rich et al, 1991) to give opening kinetics similar to phosphorylated wild-type CFTR but with less stable open channels (Lewis et al., 2004).

Lewis et al., (2004) reported that the structural and thermodynamic observations suggest that the ΔF508 mutation causes no substantive defect in the folding of NBD1.

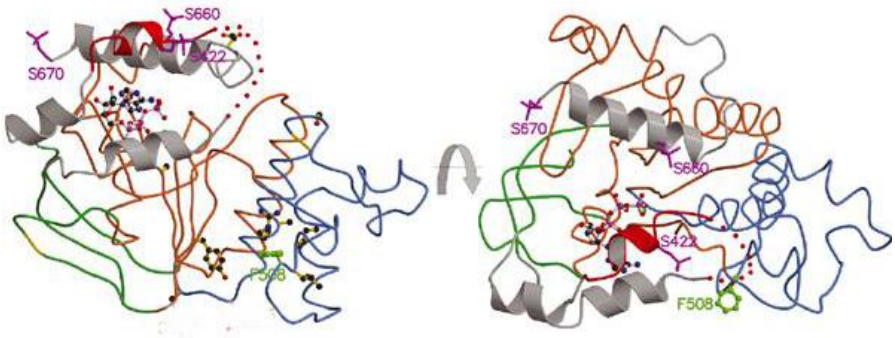

Fig. 11 Backbone structure of mNBD1 illustrating the (homologues) sites that in the human sequence are phosphorylated or CF-mutated. Left: stereo ribbon diagram of mNBD1. ATP is represented in the ball-and-stick model. Right: the same structure rotated 80° toward the viewer. Helices of regulatory segments are drawn as ribbons; the remaining polypeptide chain is a "worm" drawing. ATP is shown in the ball-and-stick model. Ser422, Ser659, Ser660, and Ser670 side chains are shown in purple (sites of phosphorylation). The amino acid span 420-428 becomes ordered upon phosphorylation (solid red). The remaining residues of the structure that were not modeled (414-419) are indicated as red dots. Side chains are shown at sites of common CF-causative mutations (Ala455, Gly480, Ile506, Ile507, Ser549, Gly551, Ala559, Arg560, Tyr569, and Asp648 colored yellow; Phe508 in green).

Interestingly, deletion of the entire RI sequence promotes maturation of F508del CFTR, perhaps because the interactions of NBD1 with the rest of the protein are positively modified (Aleksandrov et al., 2001). The regulatory extension (RE), defined by residues 638-670, has also been described as part of NBD1 (Lewis et al., 2004; Thibodeau et al., 2005). This region contains two serine residues (660 and 670) that form part of phosphorylation motif phosphorylated by PKA. It is, however, disputable whether to include the RE as part of NBD1 or of RD (Moran, 2014).

The RD domain (of around 200 amino acids) is predicted to be highly unstructured (Ostedgratd et al., 2001) and distinguished primarily by a conserved set of phosphorylation sites (12 serines; 8 threonines), which likely control the activation state of the channel (Hegedus, 2006; Riordan, 2008) through the phosphorylation by PKA (Rich 1991; Ma et al.,1997; Chang et al., 1993). In a fully phosphorylated protein, eight phosphoserines have been detected by mass spectrometry (Neville et al.,1997; Townsend et al., 1996) and NMR (Baker et al., 2007). There are several lines of evidence that suggest that not all sites contribute equally to the channel regulation. Mutagenesis of serines 660, 737, 795, and 813 cause a great reduction in channel activity, and a further reduction occurs when serines 686, 700, 712, 768, and threonine 788, are replaced (Wilkinson et al., 1997). However, it has also been proposed that phosphorylation of serines 737 and 768 could play an inhibitory rather than a stimulatory role (Vais et al., 2004; Csanády et al., 2005).

5 - Cystic fibrosis: therapeutic strategies

Life expectancy of CF-affected individuals has improved substantially in recent decades, the patient mean survival age being increased from around 14 to approximately 40 years old in Countries with well-funded healthcare systems. This has been possible thanks to early diagnosis, specialized care centers, and improved symptomatic therapies (Becq et al., 2011). In addition to relieve symptoms of the disease (with antibiotics, anti-inflammatory agents, mucolytics, nebulized hypertonic saline, and pancreatic enzyme replacement), therapeutical strategies have mainly addressed the issue of re-establishing CFTR functionality by gene therapy or use of small organic compounds, which either correct CFTR processing (principally the F508del mutant) and/or to potentiate CFTR channel activity.

Thus correctors and potentiators try to tackle the various defects in the folding, plasma membrane targeting, surface stability, and channel function of CFTR mutants (Rowel and Verkman, 2014). All this claims for a better understanding of drugs specification and of the interaction between drugs and the defective CFTR. This would also bring a beneficial reduction of off-target effects. In this respect, several attempts have been made to probe directly the efficacy of a drug (corrector or potentiator). For example, yellow fluorescent protein (YFP) mutants have been constructed whose fluorescence is strongly quenched by iodide (that is efficiently transported by CFTR) (Jayaraman et al., 2000). This is the case of the YFP mutant YFP-H148Q/I521L (Galietta et al., 2001). Hence, its co-expression with CFTR (WT or mutant) can reveal whether a specific molecule impinges on the channel activity of defective CFTRs (Pedemonte et al 2011).

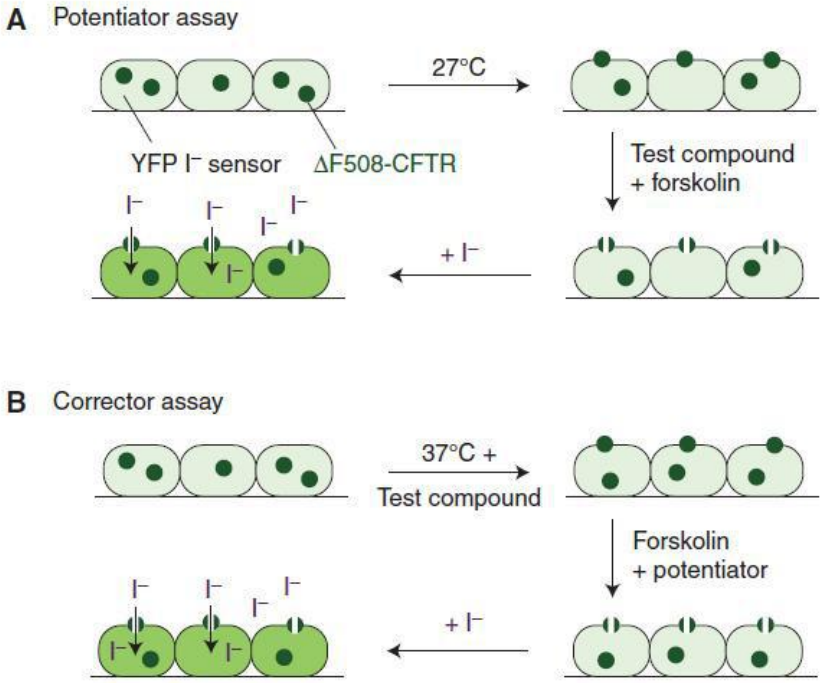

Fig. 12 High-throughput cell-based screening assays for identification of F508del-CFTR potentiators and correctors. (A) Potentiator assay. Fisher rat thyroid (FRT) cells coexpressing human F508del-CFTR and the halide sensing yellow fluorescent protein (YFP) are incubated (27 °C, 18-24 h) before assaying the presence of F508del-CFTR at the plasma membrane. Test compounds are added (10 min) in the presence of a cAMP agonist (forskolin) before iodide (I^-) addition, and F508del-CFTR function is assayed in a plate reader from the kinetics of YFP fluorescence quenching following iodide addition. (B) Corrector assay. Cells are incubated with test compounds (37 °C, 24 h). F508del-CFTR function is assayed by iodide addition in the presence of forskolin and a potentiator (e.g., genistein) (Pedemonte et al 2011).

Molecules have thus been tested to rescue the processing and trafficking defects of F508del-CFTR, and generally analyzed by high-throughput screening assays (Fig. 12), expecting that they could improve defects of the mutant-CFTR by interacting with the protein itself, or one or more of the multiple CFTR-interacting proteins that regulate CFTR biosynthesis (Becq et al., 2011). In this way, Kalid et al. (2010) were capable to identify 15 compounds (out of ~500 tested), which act as folding correctors.

Much attention was given to the potentiator VX-770 (Ivacaftor, Fig. 13, left panel) and the corrector VX-809 (Lumacaftor, Fig. 13, right panel) (Baroni et al., 2014). The former molecule seems to interact with the F508del mutant and with other less frequent CFTR mutants (e.g., G551D), in light of the improved Cl^- transport and lung function of patients bearing the G551D mutation (Ramsey et al. 2011). Instead, VX-809 increases the cell surface density of F508del- CFTR *in vitro* (Van Goor et al., 2011). However, despite many efforts on analyzing the effect of these two compounds under different conditions, the molecular basis of their interaction with CFTR, and the possible side effects, are still ill-defined. To this end, studies carried out by Baroni et al., (2014), using small-angle X-ray scattering with synchrotron radiation, to determine the electron density profile of the bilayer wall of homogeneous large unilamellar vesicles, have clearly indicated that both VX-770 and VX-809 could cause unwanted side effects because they destabilize the lipid bilayer and, possibly, cell membranes.

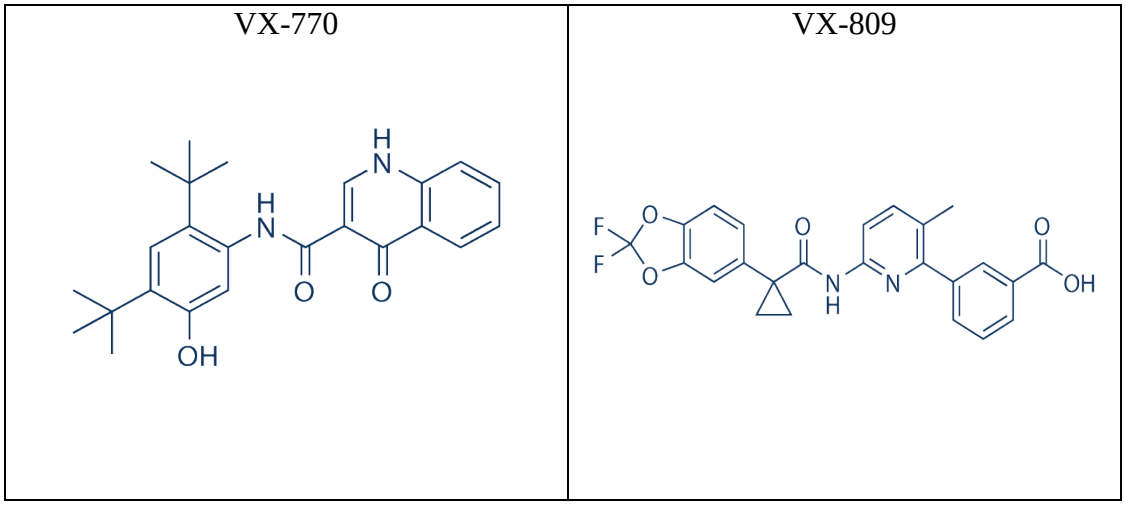

Fig. 13 The potentiator VX-770 (Ivacaftor) (left) and the corrector VX-809 (Lumacaftor) (right).

II - Materials and methods

This Ph.D. work has studied RD and NBD domains of CFTR after their production by recombinant techniques. The following sections report the procedures to obtain the proteins, some biochemical assays performed on them, and the methodologies used to study their structural features.

6 - Production and purification

6.1 - RD

We found several difficulties to produce and purify the protein. However, after many attempts, we eventually could establish protocols allowing us to generate considerable RD amounts (> 30 mg) in a high pure form (> 98%). *Escherichia coli* BL21(DE3) was transformed with a plasmid encoding the human RD isoform (from residue 654 to residue 838). The construct, generously provided by Rhea Hudson (SickKids Hospital, Toronto, Canada), was inserted into the pPROEX vector. It contained the Lac operon for its inducible expression, and a pTrc promoter. A sequence coding for an hexa-histidine sequence, necessary for purifying the protein by affinity chromatography, was included at the 3'-terminus of the RD cDNA. A stock of the transformed bacteria was stored (at -80 °C) for further utilization. A transformed *E. coli* aliquote was then inoculated in 50 ml of Luria Broth (LB) growth medium supplemented with antibiotics (chloramphenicol 1 mM, and ampicillin 0.4 mM), and bacteria were allowed to grow overnight. The following day, the culture (diluted to 1.2 lt with LB) was grown at 37 °C under stirring until reaching an optic density of 0.5 at 600 nm. Protein synthesis was induced by the addition of 1 mM isopropyl-β-D-1-thiogalactopyranoside (IPTG); after 3 h bacteria were harvested and treated with the below-described protocols to isolate inclusion bodies (IB) and the desired protein (Protocol A), and to purify the protein (Protocol B).

Protocol A

1) Suspension of cells in a buffer containing 100 mM Tris-HCl (pH 8), 2 mM EDTA, 10 mM dithiothreitol (DTT).

2) Sonication (4 °C) and centrifugation (7,500 rpm, in a Beckman JA 25-50 centrifuge, 15 min, 4 °C).

3) 5x Washings of the IB-containing pellet in a buffer containing 50 mM Tris-HCl (pH 8), 0.5 Triton-X 100, 100 mM NaCl, 1mM Na-EDTA, 1 mM DTT, followed by homogenization (using a Potter homogenizer).

4) Centrifugation (7,500 rpm, 15 min, 4 °C) and washing of the resulting pellet with a buffer containing 50 mM Tris-HCl (pH 8), 2M urea, 2 M NaCl, 10 mM DTT.

5) Centrifugation (7,500 rpm, 15 min, 4 °C) and washing of the pellet with a buffer containing 100 mM Tris-HCl (pH 8), 2 mM Na-EDTA, 10 mM DTT.

After another centrifugation, the pellet was washed again, and finally re-suspended in 10 ml of a buffer containing 100 mM Tris-HCl (pH 8), 6 M guanidinium, 5 mM imidazole, 1 mM DTT, and left overnight at room temperature. The obtained protein suspension was then subjected to affinity chromatography using a Ni-bound column (HisTrap, Ge-Healthcare Uppsala, Sweden) to purify recombinant RD, following the below protocol.

Protocol B

1) Two connected Ni-bound columns (5 ml each) were washed with (in sequence): H_2O (3 volumes), 10 volumes of "charge buffer" (50 mM $NiCl_2$), H_2O (3 volumes), 3 volumes of Buffer A (100 mM Tris-HCl (pH 8), 6 M guanidinium, 500 mM imidazole), 5 volumes of Buffer B (100 mM Tris-HCl (pH 8), 6 M guanidinium, 5 mM imidazole).

2) After adding the protein samples to the columns, their elution (at a flow rate of 1 ml/min) was accomplished with (in sequence): 10 volumes of Buffer B, 10 volumes of 5% Buffer A, and 3 volumes of Buffer A.

To identify RD-containing fractions by molecular mass (expected mass, 24 kDa, see Paper 3, Fig. 2) samples were firstly de-salted (desalting column, GE-Healthcare) to avoid guanidinium precipitation, and then subjected to SDS-PAGE (15% acrylamide). Selected fractions were then purified by gel filtration chromatography (Superdex-75 10/300 GL column, GE-Healthcare). The highest peak of the chromatogram corresponded to RD (with purity of around 90%) as routinely assayed by SDS-PAGE. To purify the protein further (up to > 98%), we used an anion exchange chromatography (HiTrap Q HP column, GE-Healthcare) that separates molecules based on net surface charges.

Due to the presence of guanidinium during purification, a denatured protein was obtained, and a three-step dialysis was necessary to achieve refolding. We firstly reduced the guanidinium concentration to 3 M in the presence of 500 mM arginine, to prevent protein aggregation (8 h, 4 °C) (Bondos and Bicknell, 2003). In the second step, the protein was dialyzed using a buffer without guanidinium but with 500 mM arginine (8 h, 4 °C), which was removed in the final step by dialysis (8 h, 4 °C) against phosphate buffer saline (PBS) (30 mM). RD was concentrated, fast-frozen in liquid nitrogen, and stored (1.5 mg/ml, -80 °C) for further use in the presence of glycerol 12.5% (to preserving it more efficiently from proteolysis in subsequent freezing and thawing steps).

The purity, quality and quantity of the final product was analyzed by SDS-PAGE (15% acrylamide), fluorescence spectroscopy, and UV absorption, respectively. A further test for the identity of the protein was carried out by Western blot (see also Paper 3). Ten-fifteen micrograms of protein were subjected to SDS-PAGE (15% acrylamide), and separated proteins were transferred to *Polyvinylidene difluoride* membranes (Millipore, Billerica, MA, USA) (1 h, 100 V, 4 °C), incubated with polyclonal rabbit anti-RD (1:1,000 Acris Antiboby GmbH, Herford, Germany) and with

horseradish peroxidase-conjugated goat anti-rabbit antibody (1:4,000, Santa Cruz Biotechnology, Santa Cruz, CA, USA), as secondary antibody. SNAP i.d.® 2.0 Protein Detection System (Millipore, Worcester, MA, USA) - according to the manufacturer's instructions - was used to perform a faster secondary antibody incubation. Immuno-detection was performed using ECL PLUS detection reagents (GE-Healthcare) and images were captured by Hyperfilm ECL (GE-Healthcare).

6.2 - NBD1 and NBD2

cDNAs coding for human NBD1 (from residue 394 to residue 672) and NBD2 (from residue 1,191 to residue 1,480) were subcloned into plasmid pT7. The NBD1-cDNA was inserted between NdeI and HindIII sites, and the NBD2-cDNA between NdeI and SalI. A hexa-histidine coding segment was included at the 3'-terminus of the open reading frame in both constructs. Protein synthesis was induced in *E. coli* BL21 (Rosetta strain, Stratagene, La Jolla, CA, USA), transformed with plasmid vectors pT7-NBD1 or pT7-NBD2, by adding IPTG (1 mM). As for RD generation, NBD1 and NBD2 accumulated in I.B. so that Protocols A and B were essentially followed with the exception that, instead of guanidinium, urea (8 M) was the chaotropic agent used in Protocol B.

Proteins were analyzed by SDS-PAGE (15% acrylamide) (expected mass: NBD1, 37.7 kDa; NBD2, 34.2 kDa) and processed by dialysis for refolding, in a three-step procedure against (PBS) containing (in sequence): 4 M urea and 500 mM arginine (8 h, 4 °C); 500 mM arginine (8 h, 4 °C); 30 mM PBS alone (8 h, 4 °C). NBD1 and NBD2 were stored separately (2.5 mg/ml, -80 °C) in the presence of glycerol 12.5%.

7 - ATP binding and ATP hydrolysis assay

7.1 - ATP binding to NBDs

Following the literature (Zoghbi et al., 2011), this parameter was determined from the quenching of the refolded protein-intrinsic fluorescence upon ATP addition. Samples containing 1.8 nM of either NBD1 or NBD2, or an isomolar NBD1-NBD2 mixture (in 100 mM Tris-HCl (pH 8.0), 5 mM MgCl2, and 1 mM DTT), and ATP concentrations ranging from 0 to 800 µM, were excited with monochromatic light at 285 nm. Uncorrected emission spectra from 305 to 400 nm were collected for each tested ATP concentration.

The apparent dissociation constant (*Kd*) was calculated by non-linear regression of the acquired data according to the equation:

$$\Delta F = \frac{[ATP]}{(Kd+[ATP])} \tag{7.1}$$

where *ΔF* is the normalized fluorescence decrease and [*ATP*] is the concentration of added ATP.

7.2 - ATP hydrolytic activity by NBDs

It was measured spectrophotometrically (25 °C) at 340 nm by following the decrease in absorbance of NADH according to the coupled reactions catalyzed by pyruvate kinase (utilizing ADP and producing pyruvate) and lactic dehydrogenase (utilizing pyruvate and NADH) (Ko and Pedersen, 1995). Samples contained 300 mM NaCl, 50 mM Tris-HCl (pH 7.5), 5 mM $MgCl_2$, 0.6 mM phosphoenolpyruvate, 0.3 mM NADH, 1.6 U of pyruvate kinase (PK), 0.5 U of lactic dehydrogenase, 25-40 µg of protein, and increasing concentrations of ATP (from 0 to 500 µM). The velocity of the reaction, v, was plotted against the ATP concentration, and was fitted according to Michaelis–Menten equation:

$$V = \frac{Vmax[ATP]}{Km + [ATP]} \tag{7.2}$$

where *Km* is the Michaelis–Menten constant, and *Vmax* is the maximum velocity of the reaction.

Parenthetically, both assays were also useful to test the correct refolding process of the NBD domains.

8 - Fluorescence spectroscopy

Fluorescence spectroscopy is a widely used technique to study the conformation of peptides and proteins (Chen and Barkley, 1998). We used this technique to assay the correct refolding of RD, NBD1 and NBD2, by following the peak-shift of tryptophan from about 365 nm (for the protein denatured state) to about 340 nm (for the protein folded state) (excitation wavelength, 295 nm). Indeed, being natural fluorophores, aromatic amino acids i.e., tryptophan, tyrosine and phenylalanine (but tryptophan is mostly exploited given its presence in most proteins) are intrinsic fluorescent probes with specific spectra, in which the position and the amplitude of the peak depends on the surrounding environment. Being hydrophobic, these residues are normally hidden inside folded proteins; however, they get exposed to the (polar) solvent upon protein unfolding and this changes the fluorescence spectrum (Callis, 1997). Instead, circular dichroism (CD) spectra (detailed afterwards) allow estimating the content of the secondary structure of a protein.

Accordingly, Fig. 14 reports fluorescence and CD spectra of purified RD in the unfolded, and folded, state. In the former case (Fig. 14A), the peak of the intrinsic fluorescence emission spectrum of unfolded RD is positioned to the red (the protein fluorophores are exposed to the environment), and it shifts to the left (by 25 nm) after refolding (the aromatic amino acids are now buried in the hydrophobic core of the protein). Also CD spectra change, revealing the increase in secondary structure content upon refolding (Fig. 14B). Even if intrinsically disordered (see afterwards), RD retains a high degree of secondary structure, as evident from the content of α-helices indicated by two minima at about 208 and 222 nm (compare the black trace of Fig. 14B to the spectrum (Fig. 15)

that a fully α-helical protein would display). Conversely, denaturated RD (grey trace, Fig. 14B) displays the typical random coil spectrum with no minima at wavelengths higher than 200 nm (for further details, see Paper 3).

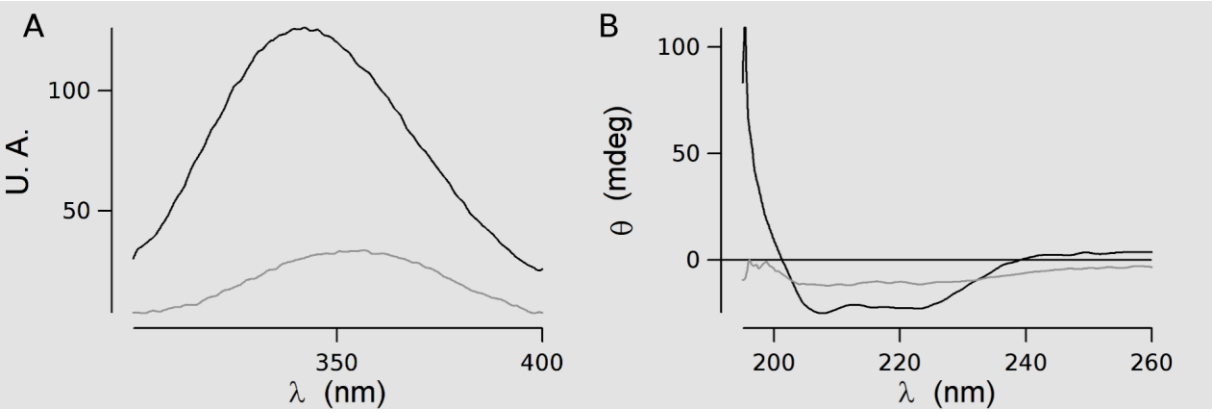

Fig. 14 Fluorescence (A) and CD (B) spectra of native (black lines) and denatured (gray) RD. A. Fluorescence emission spectra were obtained using the excitation wavelengths 274 nm to reveal the tyrosine and phenylalanine intrinsic fluorescence U. A., Arbitrary Units. B. The far-ultraviolet (UV) CD spectra were measured from 197 to 260 nm. θ = ellipticity per residue.

9 - Circular dichroism

CD spectroscopy is a technique that analyzes chiral molecules of all types and sizes in a wide range of wavelengths. It is also exploited to study biological molecules, given that it permits to observe if and how the secondary structure changes in relation to environmental conditions (temperature, pH, etc.), or upon interaction with other molecules. Important structural, kinetic and thermodynamic information can thus be obtained.

CD is based on the difference in the absorption of left-handed and right-handed circularly polarized light, a phenomenon occurring in molecules containing one or more chiral chromophores that absorb light. Because spectra of biological molecules in the far UV regions are dominated by the n π^* and π π^* transitions of amide groups, and are influenced by the geometry of the polypeptide backbone, spectra reflect the different types of secondary structures present in a protein (and thus the ϕ, ψ angles) (Whitmorea and Wallace, 2008).

9.1 - Circular dichroism and biological molecules

Proteins and peptides are composed by a sequence of amino acid residues (primary structure) that are spatially organized to provide the secondary structure, α-helix, β-sheet or turns. This specific organization and orientation of amino acids causes in the far-UV a characteristic CD phenomenon (Fig. 15):

1. α-helices have a maximum at about 195 nm and two minima at 208 and 222 nm.
2. β-sheets have a maximum at about 195 nm (but the intensity is lower than in α structures) and a minimum at 216 nm.
3. random coils have a minimum at about 200 nm.

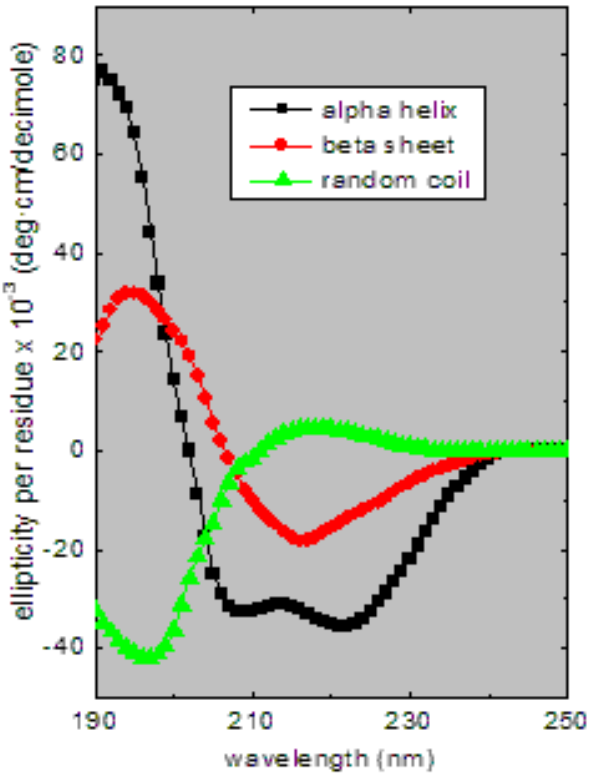

Fig. 15 CD spectra of secondary structures: α-helices (black), β-sheets (red) and random coil (green).

The CD spectrum of a given protein is the weight sum of the spectra of each secondary structure, and it thus depends on the fraction contributed by each of them. To estimate the quantity of each secondary structure present in a protein, it is necessary to deconvolve the signal:

$$\theta = f_\alpha \theta_\alpha + f_\beta \theta_\beta + f_{RC} \theta_{RC} \tag{9.1}$$

where θ_α, θ_β and θ_{RC} are the ellipticity of a spectrum of pure α-helix, β-sheet or random coil, respectively, and f_α, f_β and f_{RC} are the fraction of each secondary structure present in the analyzed protein.

Practically, for the CD experiments carried out in the present work, spectra were collected using a Jasco J-815 spectropolarimeter, equipped with a Peltier device for controlling the sample temperature, and a 0.1 cm rectangular cell. Scans were collected from 195 nm to 260 nm (at 50 nm/min rate) with a data pitch of 0.1 nm. Usually, 10 replicate spectra for each sample were

collected (at 10 °C), and normalized to the protein concentration (evaluated at 280 nm) determined immediately before each CD measurement. Analysis of the secondary structure was carried out using the on-line program Dichroweb (Whitmore and Wallace, 2008) and the algorithm SELCON3 (Sreerama and Woody, 2004).

10 - Stability of CFTR intracellular domains

Two means were used to measure the structural stability of purified intracellular CFTR domains: the first one consisted in following by fluorescence spectroscopy the denaturation of the protein by a chaotropic agent (Pace and Shaw, 2000); the second one was performed studying the thermodynamic properties of the system. Indeed, for every protein, an increase in temperature induces a transition from a native state (N) to a denaturated state (D) that depends on the physical-chemical properties of the protein and of the solution (ionic strength, viscosity, divalent cation concentration, among others) (Cortijo et al., 1988; Barone et al., 2006; Salvador et al., 2005).

10.1 - NBDs

Denaturation of NBDs (0.2- 0.5 mg/ml) was performed by the chaotropic agent guanidinium, in 50 mM phosphate buffer (pH 8.0), 1 mM DTT and 5 mM $MgCl_2$. Tests were carried out also in the presence of the potentiator 2-pyrimidin-7,8-benzoflavone (PBF) (12.5-200 nM in DMSO) (with or without 2 mM ATP), and in this case controls were performed in the presence of DMSO.

Fluorescence emission spectra (between 310 and 410 nm, excitation at 290 nm) were accumulated. The fraction of denaturated protein as a function of the guanidinuim (*Gd.HCl*) concentration was estimated from the least square fit of the spectra:

$$F([Gd.HCL], \lambda_{em} = Xd \times F(6M, \lambda_{em}) + (1 - Xd) \times F(0, \lambda_{em}) \quad (10.1)$$

where $F([Gd.HCl], \lambda_{em})$ is the fluorescence intensity at a given guanidinium concentration; $F(0, \lambda_{em})$ and $F(6M, \lambda_{em})$ are the fluorescence spectra of the native and denatured protein, obtained at 0 and 6

M guanidinium, respectively; X_d is the molecular fraction of the unfolded protein. The apparent free energy transition difference, ΔG_d, from the native to the denaturated state, at a given denaturant concentration, can be defined as (Pace and Shaw, 2000):

$$\Delta Gd = -RTln\frac{Xd}{1-Xd} \quad (10.2)$$

10.2 - RD

10.2.1 - RD sample preparation

Phosphorylation assay - To allow different RD phosphorylation levels, 100, 200 or 600 units (per 1 nM of RD) of the catalytic PKA subunit were added to the samples (final volume 20 µl) containing RD, ATP (50 µM) and $MgCl_2$ (5 mM). After incubation (30-40 min., 37 °C), the mixture was diluted (to reach an RD concentration of 0.1-2 mg/ml) using a phosphate buffer (30 mM, pH 8.0) and β-mercaptoethanol (1:3,000) that, as reducing agents, prevents possible aggregation of proteins by disulfide bonds during experiments (Bondos and Bicknell, 2003).

De-dephosphorylation assay - Alkaline phosphatase (100 units/µg of protein) was added with RD in a buffer containing $ZnCl_2$ (0.2 mM**),** NaCl (1 M), $MgCl_2$ (5 mM) and β-mercaptoethanol (1:3,000), and incubated (30 min, 30 °C).

10.2.2 - RD denaturation

Denaturation of RD was accomplished by increasing the temperature and was followed by CD that provides spectra characteristic for native and denaturated proteins. CD allows evaluating the fraction of the secondary structure content of a protein, by following (at a fixed wavelength) changes in ellipticity as a function of temperature (Fig. 16). Ellipticity is usually monitored as the minimum wavelength of the α-helix structure, θexp,222(T), because this is the secondary structure that changes most during denaturation.

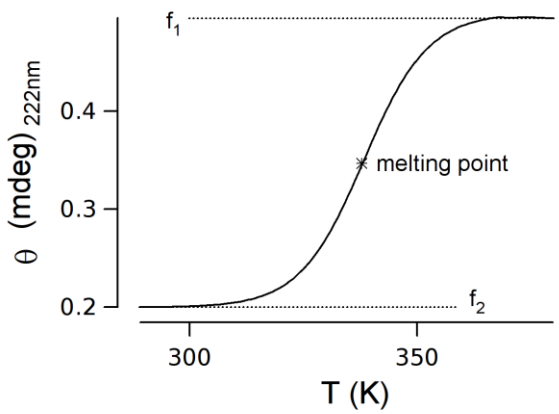

Fig. 16 Model of protein transition – from the native to the denaturated state - by monitoring ellipticity at 222 nm as a function of temperature (in Kelvin, K).

Ellipticity depends on the protein concentration, and at each temperature the ellipticity of a protein in the native state, $\theta_{N\lambda*}$, will be proportional to the fraction of molecules in this state $X_N(T)$. Likewise, ellipticity associated to denaturated molecules will be correlated to $X_D\ (T)$. Ellipticity of each state, $\theta_{D\lambda*}$ and $\theta_{N\lambda*}$, can be related to the collected experimental signals:

$$\theta_{protein\ \lambda^*}(T) = X_N\ (T)\theta_N(T) + X_D\ (T)\theta_D(T) \qquad (10.3)$$

Assuming that at the initial temperature, T_0, all molecules are in the state N, it is possible to obtain the probability of the protein to be in the native state, or in the denaturated state:

$$\theta_{protein\ \lambda^*}(T_0) = \theta_{N\lambda^*}(T_0) \quad \text{with} \quad X_N(T_0) = 1 \text{ and } X_D\ (T) + X_N(T)=1 \qquad (10.4)$$

In our experiments, denaturation curves were obtained by monitoring the mean residue ellipticity at 222 nm in the temperature range 20 °C - 95 °C, and by assuming a two state model defined as the initial native state and the final, denaturated state.

The experimentally obtained curve (at the selected wavelength $\theta_{exp,\lambda*}(T)$) is fitted with a sigmoid function (Tello-Solís and Romero-García, 2001; Sanchez-Ruiz and Martinez-Carrion, 1988),

$$\theta_{exp\lambda}*(T) = \frac{f_1+f_2}{1+exp^{\frac{T-Tm}{f_3}}} + f_1 \qquad (10.5)$$

where T is the absolute temperature, T_m is the melting temperature (point) (at which $X_D = X_N$), f_1 and f_2 are the asymptotic maximum and minimum values, respectively, and f_3 is the e-fold slope of the curve (see Fig. 16). Assuming that at T_0 all molecules in solution are in the native state, N, the fraction of molecules that get denaturated as a function of temperature, $X_D(T)$, will be estimated by normalizing the experimental curves using the parameters in equation 10.5:

$$X_D(T) = \frac{\theta_{exp\lambda^*}(T) - f_1}{f_2} \tag{10.6}$$

In addition, the fraction of molecules in the native and denaturated state are related to the standard free Gibbs energy by the ratio of their respective concentration (X_D/X_N)**:**

$$\Delta G^0(T) = RTln(\frac{X_D}{X_N}) \tag{10.7}$$

where ΔG^0 is the standard Gibbs free energy difference between the initial and final states and R is the gas universal constant.

Finally, because of the relation between enthalpy (ΔH) and entropy (ΔS) variations:

$$\Delta G^0(T) = \Delta H - \Delta S \tag{10.8}$$

combination of equation (10.8) with equation (10.7) allows to obtain the Van't Hoff equation:

$$ln\frac{X_D}{X_N} = \frac{1}{T}\frac{\Delta H}{R} - \frac{\Delta S}{R} = \frac{1}{RT}\Delta G^0(T) \tag{10.9}$$

All this to explain that, by using the above equations on normalized experimental data, one can describe the denaturation process of a given protein, and, hence, characterize its stability.

10.2.3 - Thermodynamic study of the native and phosphorylated RD

The CD methodology used for RD was as described earlier (page 9). Also, as mentioned, RD denaturation curves (obtained by monitoring the mean residue ellipticity at 222 nm, θexp,222(T), as a function of temperature (from 20 to 95 °C) were analyzed assuming a two state model, defined as the initial native state and the final, denaturated state (Sanchez-Ruiz and Martinez-Carrion, 1988; Tello-Solís and Romero-García, 2001). To identify the initial and final states, the experimental θ*exp*,222(*T*) curves were first fitted with a sigmoid function (equation 10.6). We normalized the curves to estimate the fraction of denatured protein, X_D according to equation 10.7. Data was fitted according to the Van't Hoff plot (equation 10.9).

11 - Small-angle scattering of X-rays experiments

Small angle X-ray scattering (SAXS) is a technique appropriate to investigate the structure of a wide range of particles in solutions, given that the provided information on the geometrical invariants of a protein allows to model a 3D structure with a resolution of around 8-20 Å. Although X-ray crystallographic studies provide a resolution at the atomic level - SAXS forwards only in the shape of a protein (Fig. 17) (Svergun and Koch, 2001) - SAXS is a good compromise for those proteins that do not crystallize, and/or when crystallographic information is not crucially necessary. In addition, SAXS offers the advantage to study proteins in solution.

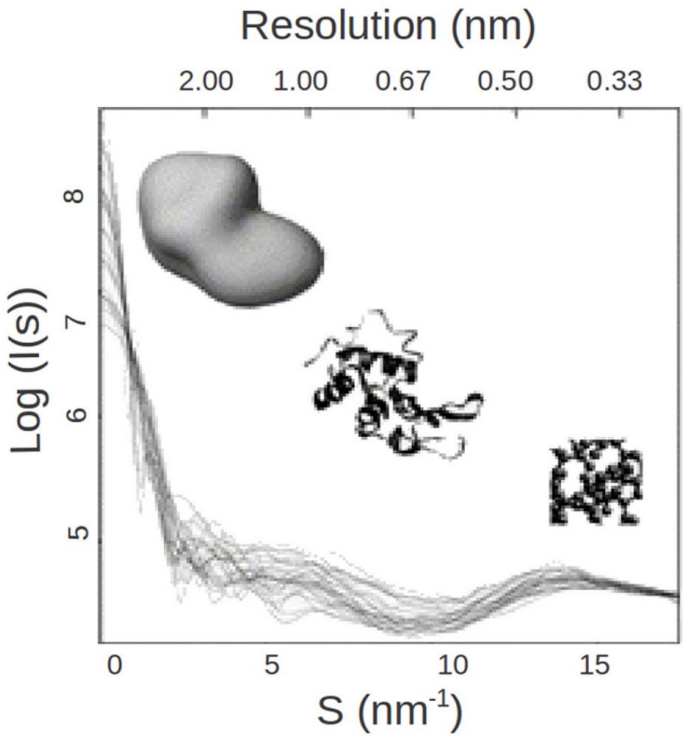

Fig. 17 Representation of the achievable resolution allowing a 3D re-construction of a protein in function of the scattering vector.

In a SAXS experiment, the sample is exposed to a monochromatic X-ray beam (typically between 0.8 to 2 nm); and the diffraction pattern is recorded by a detector. The intensity of the emitted radiation is calculated by integrating the signal recorded in each circle inside the detector (Fig. 18). After appropriate geometrical corrections of the parallax, the scattered intensity *I(s)* (equation 11.4) is plotted as a function of momentum transfers:

$$s = \frac{2sin\theta}{\lambda} \tag{11.1}$$

where θ is the angle between the incident and scattered radiation (Fig. 18). The total amplitudes of the scattering radiation (equation 11.2) should be the sum of scattered waves. However, considering that the distance between the detector and the sample is much greater than the inter-atomic distances, it is not possible to separate the contributions of individual electrons (Fig. 18).

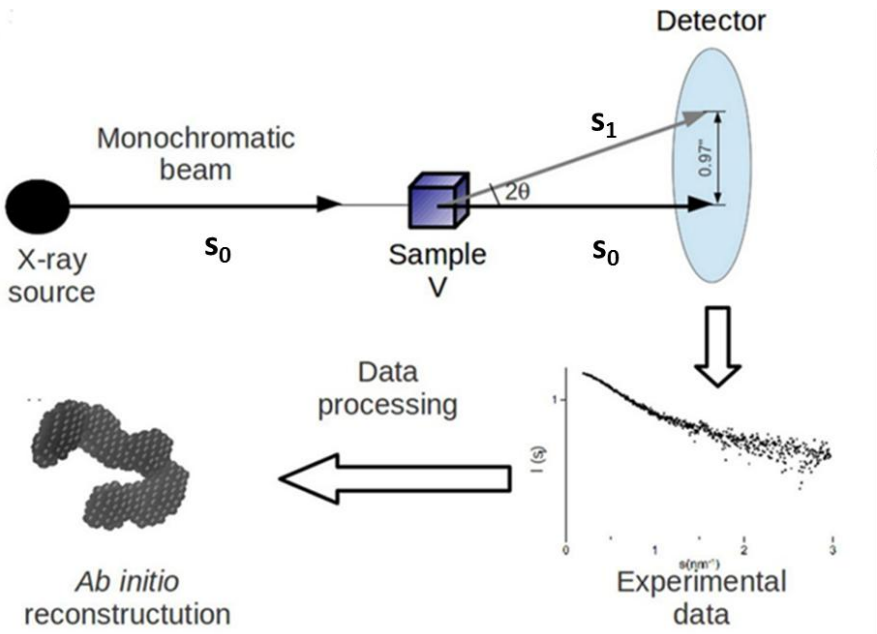

Fig. 18 Scheme of a SAXS experiment allowing reconstruction of the shape of a protein (for the used symbols, see text).

The total amplitude of scattering radiation $F(s)$ is:

$$F(s) = \int_{Vr} \Delta\rho(r) e^{-2\pi r \cdot s} dVr \quad (11.2)$$

where V_r is the volume of the sample and s is the scattering vector, defined as the difference between the vector of the incident beam, s_0, and the vector of the scattered wave, s_1, (see Fig. 18) and $\Delta\rho(r)$ (called contrast) is defined by the difference between the electron density of the particle, $\rho(r)$, and that of the homogeneous solvent, ρ_0.

$$\Delta\rho(r) = \rho(r) - \rho_0 \quad (11.3)$$

The intensity recorded, $I(s)$, is the square of the total amplitudes of the scattering radiations (equation 11.2):

$$I(s) = |F(s)|^2 \quad (11.4)$$

In the case of SAXS, the size and shape of the particles in solution are homogeneously distributed, and therefore we can assume that the solution is mono-dispersed. To get information about the shape and the dimensions of CFTR domains in solution, we analyzed SAXS spectra using the Guinier approximation (Feigin and Svergun, 1987; Guinier and Fournet, 1955). Accordingly, an example of the data range - indicated in the Fig. 19 - as that part of the curve in evidence by the orange circle - from the collected SAXS spectra, used to perform analysis by Guinier plot (Guinier and Fournet, 1955).

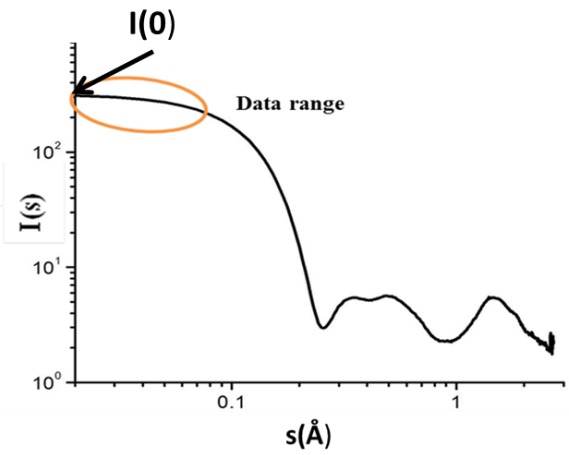

Fig. 19 The slope of the SAXS spectra (indicated in the circle) gives information about the shape and the dimension of the molecules in solution. *I*(0) is the intercept of the curve with *I*(*s*).

11.2 - Samples preparation for SAXS experiments

11.2.1 - RD

For RD samples preparation see paragraph **10.2.1.**

11.2.2 - NBDs

Protein samples containing NBD1 and NBD2 alone or an equimolar NBD1/NBD2 mixture (1.2-1.8 mg/ml), were prepared in a phosphate buffer (50 mM, pH 8.0). When required, samples were supplemented with 2 mM ATP or 25 nM PBF.

11.2.3 - SAXS spectra

SAXS spectra were carried out using native and phosphorylated *RD* samples, or NBDs samples containing each domain alone, or an equimolar mixture of them. Beforehand, samples were cleared using a 0.45 µm filter (Ultrafree-MC, Millipore), and concentrated by ultrafiltration with an Amicon membrane. Sample protein concentrations were determined from the absorbance at 280

nm. Each protein sample was subjected to dialysis (buffer phosphate, 30 mM), the dialysis buffer being used to measure SAXS background signal.

Spectra were collected at the ID14-EH3 beam line of the European Synchrotron Radiation Facility (ESRF, Grenoble). The distance of the detector (1.83 meters) covered the range of the momentum transfer $0.08 < s < 3.6\text{-}4.5$ nm-1 (using a wavelength = 0.093 nm); X-ray optical path through the sample was about 1 mm. Data were collected at 10 °C. For each sample, ten spectra of 30 s each were recorded, for a total of 5 min of acquisition. When using RD samples, glycerol (1.5%) was present to scavenge free radicals and thus to minimize possible radiation damages to the protein. Instead, when using NBDs samples, DTT (1 mM) was added to prevent anomalous S-S formation during the experiment (Bondos and Bicknell, 2003).

A comparison of the 10 successive exposures showed no change in the scattering patterns, suggesting that no measurable radiation damage to the proteins had occurred. Sample protein concentrations were normalized to the intensity of the transmitted beam, and the scattering data from the buffer dialysis (performed before and after each measurement, see above) was averaged and used to subtract the background.

11.3 - Analysis of SAXS experimental data

In this work, most of SAXS data analysis were done with the software package ATSAS, developed by D. Svergun's group at EMBL outstation of Hamburg (www.embl-hamburg.de/biosaxs).

11.3.1 - Guinier approximation

The Guinier approximation can be applied close to the origin of the SAXS spectra (Fig. 19) in a mono-disperse solution. The scattered intensity $I(s)$ can be approximated by a Gaussian where the width is proportional to the square of the radius of gyration, R_g. In practice, a linearized representation can be used, by plotting $\ln(I(s))$ vs s^2 (Guinier plot), to obtain, by a linear fit, an estimation of $I(0)$ and of R_g of the protein in solution.

$$I(s) = I(0)e^{(\frac{4\pi^2}{3}Rg^2s^2)}$$
$$\ln(I(s) = \ln(I(0) - \frac{4\pi^2}{3}R^2{}_g s^2 \quad (11.5)$$

where $I(0)$ is the intensity at zero angle and R_g the radius of gyration.

The Guinier approximation is valid only for the s-values that respect the condition:

$$sR_g < 1.3 \quad (11.6)$$

R_g value, determined by analyzing SAXS data, is related to the mass of the molecules in solution.

In addition to apply the approximation in the appropriate angular range (according to the condition (11.6), the Guinier approximation relies of an ideal mono-disperse solution. A bad Guinier plot is a strong indicator of a poor quality of the sample. Improper background subtraction, presence of attractive or repulsive inter-particle effects and sample poly-dispersity result in deviations of the interpolated curve.

A correlation exists between R_g and the geometrical radius, as shown in Fig. 18

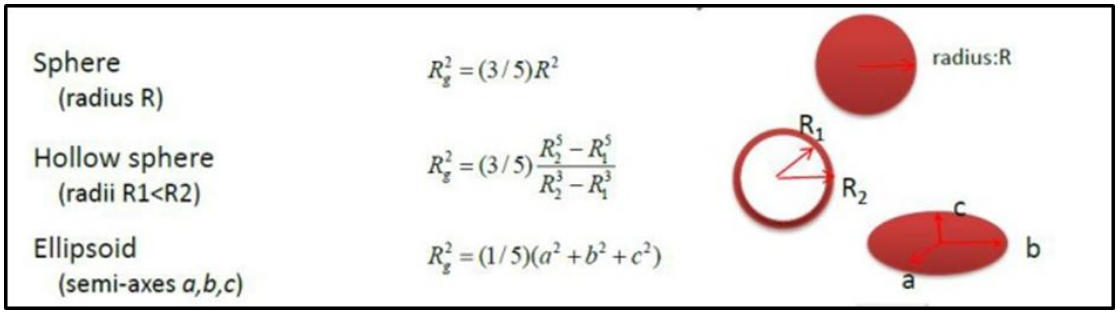

Fig. 20 Radius of gyration of some homogenous bodies in solution.

11.3.2 - Molecular mass determination

The intensity at zero angle (obtained by the Guinier approximation) is proportional to the molecular mass M of the scattering particle. A known standard protein (usually bovine serum albumin) is measured to estimate the molecular mass of the protein of interest using the relation (Mylonas and Svergun, 2007):

$$M^{(sample)} = I(0)^{sample}\ \frac{C^{(standard)} M^{(standard)}}{I(0)^{standard}\ C^{(standard)}} \qquad (11.7)$$

where *M*(*sample*) is the molecular mass of the sample, *M*(*standard*), *C*(*standard*), and *I*(*0*)(*standard*) are the molecular mass, the concentration and the intensity at zero angle of the standard protein, respectively (Mylonas and Svergun, 2007).

However, because of the limitations inherent to the Guinier approximation, albeit indirectly, values of *Rg* and *I*(*0*) can be derived from the Fourier transform methodology. Fourier transformation of the scattering intensity yields the distance distribution function *P*(*r*):

$$P(r) = \frac{r^2}{2\pi^2} \int_0 s^2 I(s) \frac{\sin sr}{sr} ds \quad (11.8)$$

and consequently

$$I(s) = 4\pi \int_0^{Dmax} P(r) s(r) \frac{\sin s(r)}{s(r)} dr \quad (11.9)$$

where D_{max} is the maximum particle diameter.

$P(r)$ is a real space representation of the scattering data and allows one to graphically display the features of the particle shape (Fig. 20). For example, globular particles yield bell-shaped profiles with a maximum at approximately $D_{max}/2$, whereas multi-domain particles often yield profiles with multiple shoulders and oscillations corresponding to intra and inter-subunit distances (Fig. 21 and 22) (Mertens and Svergun, 2010).

In equation (11.8), $P(r)$ takes in account an ideal system. Conversely, in an experimental setup the intensity ($I_{exp}(s)$) is not determined by an infinite angular range but by a restricted one $s_{min} < s < s_{max}$ (Feigin and Svergun, 1987), impeding therefore to calculate $P(r)$ from the Fourier transformation (equation 11.8, 11.9) of $I_{exp}(s)$ from a finite number of points. Hence, the Fourier transformation is calculated indirectly (Glatter, 1977), and the program GNOM (Svergun, 1992) has been designed accordingly.

GNOM is an indirect transform program for small-angle scattering data processing. It reads scattering curves in one-dimension (possibly smeared with instrumental distortions) and evaluates the particle distance distribution function $P(r)$ (for mono-disperse systems) or the size distribution function D(R) (for poly-disperse systems) (Svergun, 1992).

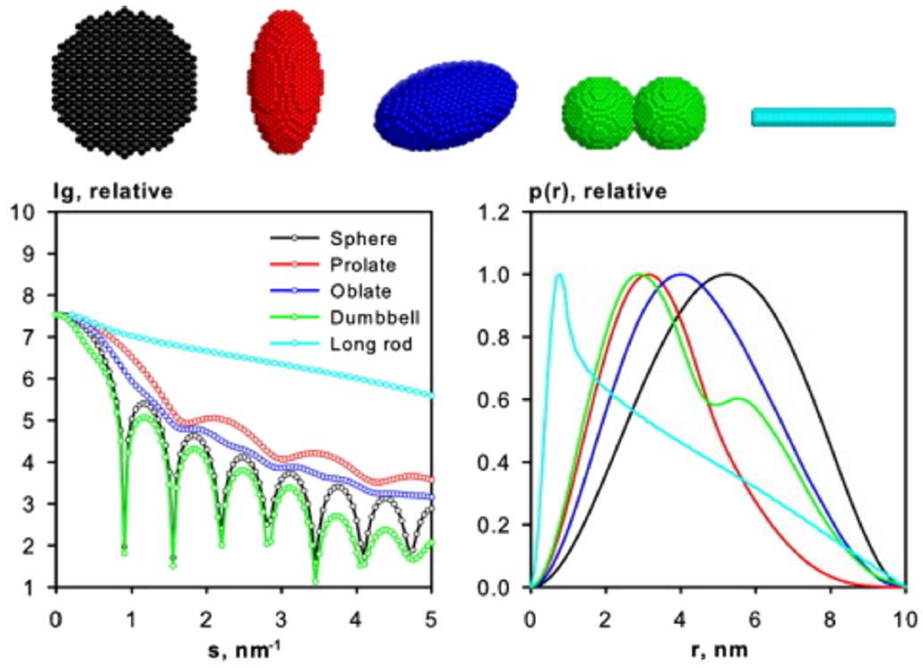

Fig. 21 Scattering intensity and pair distribution functions of five kinds of protein shape according to the Fourier transform methodology.

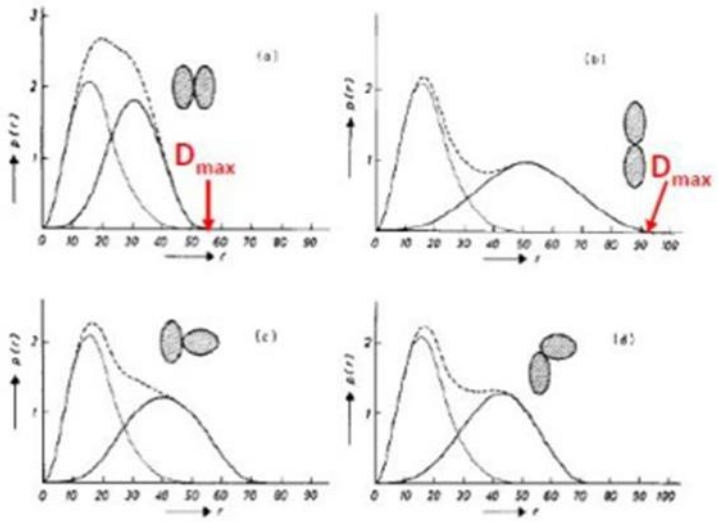

Fig. 22 Schematic representation of a dimer in solution and the different conformational changes in relation with *P(r)* and D_{max}, following the Fourier transform methodology. Graphs, showing the distribution of distance, underline the mass centre of each monomer and their reciprocal position in the dimeric configuration.

11.3.3 - Krakty Plot

Information on the folding of proteins in solution can be obtained by a graphical representation of the experimental data, named Kratky plot. By plotting I(s) xs^2 against s, one can argue the folding state (Fig. 23) in which: (i), globular proteins typically yield a prominent peak at low angles (curve 1); (ii), unfolded proteins a continuous increase of the relation (curve 2); (iii), partially unfolded proteins, yielding a mixture of curves 1 and 2 (curve 3), which is also similar to the behavior of flexible multi-domain proteins.

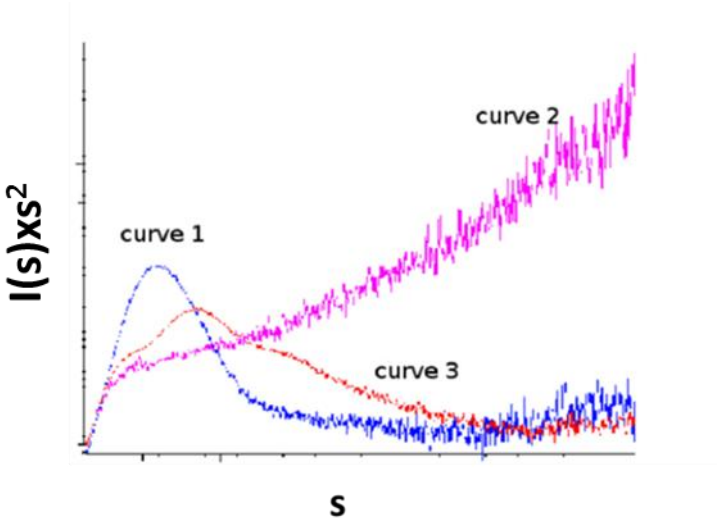

Fig. 23 Kratky plots of three proteins with different folding: globular (curve 1), denaturated (curve 2), partially unfolded (curve 3) (for used symbols, see text).

11.3.4 - Porod invariant

Higher s values of the SAXS spectra contain information on the shape of a molecule. By assuming a uniform electron density inside the particle, the volume (*V*) is estimated following the Porod's equation (Porod, 1982):

$$V = \frac{2\pi^2 I(0)}{Q} \qquad Q = \int_0^\infty s^2 I(s) ds \tag{11.10}$$

The estimation of *V* permits an alternative way to obtain the mass of a molecule, in which I(0) is the intensity of the scattering sample at zero angle, and Q the Porod invariant (Porod, 1982).

11.3.5 - *Ab initio* reconstruction models of proteins

A 3D reconstruction of a protein shape can be obtained following SAXS data. Given that information by scattering data is drastically reduced by the random orientation of particles in solution, data interpretation is usually performed in terms of homogeneous and rigid bodies.

An *ab initio* method, to reconstruct the 3D structure of molecules for which only low-resolution data are available, is based on automated bead-modelling first proposed by Chacon et al. (1998).

The programs used here to this purpose are now briefly outlined.

DAMMIN (Dummy Atom Model Minimization) (Svergun, 1999)**.** This program envisages that the volume enclosing a particle (e.g., a sphere of sufficiently large radius) is filled with N densely packed spheres of radius r, referred to as dummy atom. Given the fixed spatial positions, the shape of the dummy atom model is described by a vector X with N components assigning each dummy atom either to the solute phase (i.e., a protein in this case) or to the solvent phase. For an adequate description of a structure, the number of dummy atoms usually reaches a few thousands. The task of shape reconstruction from the scattering data is thus to find a configuration X where a goal function f(X) is minimized. The goal function takes into account the discrepancy between the experimental data and the calculated scattering of the dummy atom model, as well as other aspects of the model (quantified as penalties). The contribution of the penalties to the goal function is expected to be 10-

50% for the final model. The obtained conformations are then classified, aligned and averaged using a suite of programs (Svergun, 1999) as following.

DAMCLUSTER is a cluster analysis of all models to find outliers from the largest group(s).

DAMSEL compares all models to find common features and eventually reject outliers.

DAMSUP aligns all models.

DAMAVER averages aligned models (Volkov and Svergun, 2003).

DAMFILT filters the averaged models at a given cut-off volume.

All the above programs minimize a normalize spatial discrepancy (NSD) to find the best alignment of two models. NSD is a measure of quantitative similarity between sets of 3D points (as explained below). For ideally superimposed similar objects, NSD tends to zero, while it exceeds 1 if the object systematically differ from one to the other (Kozin and Svergun, 2001). NSD is calculated as follows (Bernadò et al., 2007). In the presence of two 3D models - represented as sets of points - the above programs are able to calculates the minimum value among the distance between every point of the first model (model 1) and all points of the second (model 2). The same procedure is applied for every point of model 2. The distances are added and normalized against the average distance between the neighboring points for the two sets.

DAMMIF Being an implementation of the above-described bead-modelling program, it rapidly determines an *ab initio* shape using small angle scattering (Franke and Svergun, 2009). Thus, starting from the DAMMIN (arbitrary) initial model, DAMMIF utilizes simulated annealing to construct a compact interconnected model yielding a scattering pattern that best fits experimental data.

EOM (EOM: Ensemble Optimization Method) It fits the averaged theoretical scattering intensity from an ensemble of conformations into SAXS experimental data (Bernadò et al., 2007). A pool of n independent models based upon sequence and structural information is first generated. For

proteins, expected to be intrinsically unfolded, no rigid bodies are required in input and completely random configurations are created based upon the sequence. Crystallographic symmetry can be exploited using either an high-resolution oligomerized domain (if present), or specifying a potential oligomerization interface on a domain. Once the pool generation is completed, an algorithm for the selection of the ensemble is conceived. Hence, the algorithm compares the averaged theoretical scattering intensity (from n independent conformational ensembles) against SAXS data. The ensemble that better describes the experimental SAXS data is then selected.

SUPCOMB This program allows to superimpose a 3D structure onto another one (Bernadò et al., 2007). Structures can be low-resolution bead models, and/or high resolution NMR, or X-ray crystal structures, but shape models are not considered. The program represents each input structure as an ensemble of points, then minimizes a NSD to find the best alignment of two models.

III - Results

12 - List of papers

The published papers (referred to by numerals 1- 4) containing the main outcomes of the Ph.D. work, are integral part of the thesis itself. In the following paragraph, however, their content will be briefly summarized.

Paper n. 1 - Galeno L, Galfrè E, Moran O. Small-angle X-ray scattering study of the ATP modulation of the structural features of the nucleotide binding domains of the CFTR in solution. Eur Biophys J 40:811-24, 2011.

Paper n. 2 - Galfrè E, Galeno L, Moran O. A potentiator induces conformational changes on the recombinant CFTR nucleotide binding domains in solution. Cell Mol Life Sci 69:3701-13, 2012.

Paper n. 3 - Marasini C, Galeno L, Moran O. Thermodynamic study of the native and phosphorylated regulatory domain of the CFTR. Biochem Biophys Res Commun 423:549-52, 2012.

Paper n. 4 - Marasini C, Galeno L, Moran O. A SAXS-based ensemble model of the native and phosphorylated regulatory domain of the CFTR. Cell Mol Life Sci. 70:923-33, 2013.

12.1 - Rationale, and main results, of Papers 1 - 4

Paper 1 reports our investigation on the structure of CFTR NBDs, which we carried out in light of previous observations suggesting that the putative binding site for CFTR drugs could be located in the NBD1-NBD2 interface (Moran et al., 2005; Zegarra-Moran et al., 2007), and on a few available data on biochemical and structural aspects of CFTR. For example, Gadsby et al. (2006) reported that CFTR channel is activated following a cAMP-dependent phosphorylation of RD, and that the ATP binding to NBDs evoked the channel gating. In addition, Vergani et al. (2005) proved that the binding of two ATP molecules to NBD1 and NBD2 triggered dimerization of the domains, and that such structural change induced the opening of the channel (see also Mense et al., 2006; Lu and Pedersen, 2000; Kidd et al., 2004)

Our strategy consisted in first following the binding of ATP to recombinantly-generated NBDs by fluorescence spectroscopy, and then in the study by the SAXS approach of the structure of the domains in solution. This allowed us to obtain clear evidence of the modulation exerted by ATP on the NBDs' conformation, specifically on the capacity of ATP to induce the tight dimerization of NBD1 (present alone), but also of the NBD1/NBD2 mixture. Conversely, dimerization of NBD2 molecules present alone could not be observed.

As reported in Paper 2, such results encouraged us to investigate on the interaction of NBDs with those drug molecules called "potentiators", which impact on the response of defective CFTR channels (belonging to class III mutations) to cAMP-dependent phosphorylation (for additional information on therapeutic drugs, please refer to chapter 3). NBDs figured out from literature to be the putative binding site of potentiators; indeed many studies have brought evidence to support the same type of the interaction mechanism between CFTR potentiators and the protein: competition has been described between genistein and benzimidazolones (Al-Nakkash et al., 2001), 7,8-benzoflavones and benzimidazolones (Caci et al., 2003) and genistein and capsaicin (Bompadre et al., 2005). Potentiators probably act by binding at the NBDs to favor the chloride permeable state of

the protein. This hypothesis is supported by the observation that mutations in conserved residues of the NBDs, such as G551D and G1349D, exhibit a shift in the affinity for potentiators (Pedemonte et al., 2005; Van Goor et al., 2006).

To identify the binding site of potentiators, we modeled the NBD1/NBD2 dimer and compared the theoretical binding-free energy of several compounds docked on the model with the experimental binding free-energy using a wild-type and two mutated (G551D and G1349D) CFTR (Moran et al., 2005). We found a good correlation between these two parameters for a putative binding site located in the interface of the NBD1-NBD2. In this way, we highlighted that a putative binding site for potentiators was located to the interface of NBD1-NBD2 dimer. This result strived us to accumulate physic-chemical and structural proofs to experimentally sustain this possibility. In particular, by performing denaturation experiments (with guanidinium) on isomolar recombinantly-generated NBD1-NBD2 mixtures supplemented with 2-pyrimidine-7,8-benzoflavone (PBF, one of the most potent CFTR potentiators), we calculated the free energy difference of the transition from native to denaturated state founding that the potentiator modifies the structure of NBD1/NBD2 increasing the denaturant accessibility, as the concentration of PBF increases. We also measured the binding of ATP to the NBD1-NBD2 dimer, and the dimer ATP hydrolytic activity with, or without, PBF: the apparent affinity of the NBD1/NBD2 complex in solution is significantly higher than that estimated in the whole CFTR (Kidd et al., 2004); moreover the apparent dissociation constant for ATP is about constant at concentrations of PBF between 0 and 200 nM.

Finally, by analyzing with SAXS the structural modifications of the NBD1/NBD2 dimer in the presence of PBF, we were able to demonstrate that PBF induces a significant conformational change of the NBDs

As reported in the Introduction section, it is still ill-defined the structure of CFTR RD, which plays a fundamental role in the channel activation following the phopshorylation of nine of its serines. We

now know that such a post-translation modification induces profound RD structural changes, as observed by both CD (Dulhanty et al., 1995) and NMR (Baker et al., 2007) studies. Likely, RD conformational changes impact on the RD interactions with NBDs (Chappe et al., 2005; Kanelis et al., 2010). Accordingly, Paper 4 reports the work carried out on the structure of recombinant RD in both the native state and after different phosphorylation events. In this study, CD was utilized to gain information on the secondary structure of the protein. By deconvoluting CD spectra, we could infer that, although more than 30% is in a disordered conformation (although not totally unfolded – see Paper 3), still native RD retains a certain amount of secondary structure (45.9% α-helix; 12.1% b-Sheets;) that, however, is significantly altered following the phosphorylation events (71.1% α-helix; 0.8% β-sheets; 18.4% random coil). Fluorescence spectroscopy was employed to better understand such a conformational change, which showed that has also shown a difference between the unfolded RD in 6 M guanidinium-HCl and the folded protein after the dialysis procedure, confirming the difference between the completely unfolded state and the native protein. These experiments have also shown an increasing of intrinsic tryptophan fluorescence, following the RD phosphorylation.

We performed Size Exclusion Chromatography (SEC) to measure experimentally the RD molecular mass; thus, comparing the RD estimated molecular mass (~24 kDa) of the protein, for both native and phosphorylated in solution, to the experimental ones, we confirm that RD is a monomer in solution and that the small partition coefficient measured by SEC is actually due

to the large Stoke radius of the protein, and not to some protein aggregation during the chromatography experiments. Moreover we obtained information about the shape of RD in solution referable to a non-globular proteins.

Finally, through data obtained by SAXS experiments, we obtained the structural model of native and phosphorylated RD: the *ab initio* molecular shape reconstructed from the SAXS data results in elongated molecules for both native and phosphorylated RD and the models confirm the molecular changes produced by the phosphorylation.

12.1.1 Paper 1

Small-angle X-ray scattering study of the ATP modulation of the structural features of the nucleotide binding domains of the CFTR in solution.

12.1.2 - Paper 2

A potentiator induces conformational changes on the recombinant CFTR nucleotide binding domains in solution.

12.1.3 - Paper 3

Thermodynamic study of the native and phosphorylated regulatory domain of the CFTR.

12.1.4 - Paper 4

A SAXS-based ensemble model of the native and phosphorylated regulatory domain of the CFTR.

IV - Discussion and conclusions

Because CF is the most common genetic disease in humans, a more complete understanding of the structural features of CF root cause, CFTR, and in particular of the intracellular domains (NBD1, NBD2 and RD) that play a key role in CFTR function, is highly needed. This type of information could shed light into the patho-physiology of CFTR and help, therefore, devising safe and effective therapeutic strategies against the disease.

For this reason, the work carried out during the 3-year doctorate course dealt with some molecular features pertaining to NBD1, NBD2 and RD, which were generated separately in bacteria, purified from inclusion bodies and refolded. In this respect, it is good to mention that quite a great effort had to be devoted to obtain an appreciable refolded state of the proteins, for which the literature helped only partially. In fact, after using several of the available protocols, we introduced a stepwise dialysis - to remove the used chaotropic agent - that gave the best, and reproducible, results.

Taken together, the conclusions of the different aspects of the work - present in Papers 1-4 - indicate that the biochemical and biophysical characterization that we obtained for the intracellular CFTR domains are such that, along with the provided low-resolution models, may likely further our understanding on the pathogenesis of CF. A brief discussion of the obtained data, and the main conclusions thereof, are now exposed as follows.

13 - Structural and biochemical features of NBD1 and NBD2

After the refolding step, recombinant isolated NBDs, and the equimolar mixture of NBD1 and NBD2, were thoroughly studied by CD and SAXS techniques.

Beforehand, however, it was necessary to test the "quality" of the refolding status of the proteins. One test was an indirect assay, i.e., the capacity to bind ATP followed by fluorescence

spectroscopy, for which more than acceptable values for dissociation constants were found: 115 µM for NBD1, 403 µM for NBD2, and 93 µM for the NBD1/NBD2 mixture (see Fig. 2b, Paper 1). Then the intrinsic tryptophan fluorescence (see chapter 2 of the thesis) of refolded NBD1 and NBD2 were compared to the denatured ones.

The final yield of refolding of NBD1 and NBD2 was between 70 and 75%. Interestingly, when an equimolar mixture of NBD1 and NBD2 was processed for refolding, the yield slightly increased to about 80% (data not shown). Moreover, we found that the addition of 2 mM ATP during refolding further increased the yield to about 80-85% (data not shown).

In order to control the refolding of NBD1 and NBD2, isolated or in an equimolar mixtures (see Fig.1c, Paper 1), proteins were analyzed by CD. In all cases, far-UV spectra revealed similar contents of secondary structures: 24% α-Helix and 25% β-Sheet, for NBD1; 20% α-Helix and 30% β-Sheet, for NBD2; 25% α-Helix and 23% β-Sheet, for the NBD1/NBD2 mixture. These values are consistent with previous findings on recombinant NBDs (Logan et al. 1994), but the contribution of β-sheets and of α-helices are higher and lower, respectively, than the values obtained from the crystallographic analysis of NBD1 and NBD2.

Although we believe that the dialysis procedure used by us to refold NBD1 and NBD2 recovers the domain's native conformations, we are unable to provide an unequivocal explanation for the discrepant results towards crystallographic data. One possible reason is the fact that analysis of CD data is not based on theoretical rigorous criteria but on a statistical comparison with other known structures by means a multi-parametric fit. Essentially, it depends on the fitting criteria. On the other hand, one has also to admit that ours would not be the first example for this type of discrepancy, given that the secondary structure detectable in proteins in solution may not axiomatically coincide with the secondary structure present in crystals (Hartman et al. 1992; Logan et al. 1994; Karpowich et al. 2001).

Use of the SAXS technique provided us, firstly, with values of the gyration radius (R_g) (referring to the mass radius and giving, therefore, information on the molecule dimension) for both NBD1 and NBD2. The first observation is that both NBD1 and NBD2, when in solution, show a globular conformation with characteristic R_g that is consistent with those reported for the NBD1 and NBD2 atomic structures obtained by X-ray crystallography; indeed, the *ab initio* reconstruction of the shape of the domains revealed an envelope hosting NBD1, or NBD2, as known from their crystallographic structure (see Fig. 5, Paper 1). This result supports, therefore, the contention that (at least) NBD1 crystal structure is probably not too different from that in solution.

NBD1 and NBD2 have a monomeric conformation, but that they form a dimer if present together in an isomolar concentration (the mass of the scattering particle being fully consistent with the heterodimer predicted mass).

We found that the SAXS pattern obtained from the NBD1/NBD2 mixture could not be described just as the sum of the properties of the single NBDs. Indeed, the deduced geometric properties are compatible with the presence of a structure bigger than that of NBD monomers, possibly with a dimer. In the absence of ATP, the *ab initio* reconstruction of the NBD1/NBD2 dimer reveals a globular structure, with two divergent ‘‘wings’’ (see Fig. 6, Paper 1). This shape is not compatible with the common head-to-tail conformation, such as that reported for NBD1 and the NBD1/NBD2 models (Moran et al. 2005; Mornon et al. 2009) or for NBDs belonging to the other ABC-proteins. The best fit of this low resolution model with the atomic structures of NBD1 and NBD2 yields a conformation that has some analogies to the Mornon’s model of the conformation of the NBDs in the closed CFTR channel (based on homologies to bacterial proteins) (Mornon et al. 2009). Indeed, the NBD1/NBD2 region of the Mornon’s model can be docked to the low resolution model of NBD1/NBD2 in the absence of ATP.

On the contrary, in the presence of ATP, NBD1/NBD2 dimer undergoes to a tight dimerization and this conformation is very similar to the crystallographic head-to-tail conformation reported for this

subunit (Moran et al. 2005; Mornon et al. 2009), as well as to the SAXS shape reconstruction of the NBD1/NBD2 dimer.

Parenthetically, SAXS allowed us to observe that NBD1 undergoes to a tight dimerization (Fig. 8a, Paper 1) while dimerization of NBD2 doesn't occurs, in the presence of ATP.

The addition of ATP changes the complex conformation - from a bi-lobular shape (in the absence of ATP) to a tight sphere (in the presence of ATP). It is important to stress that, rather than inducing the dimerization process, ATP produces a small conformational change in the relative positions of NBD1 and NBD2 that could be correlated with the channel gating of CFTR (Vergani et al. 2005).

From the biochemical point of view, our experiments confirmed (see, Ko and Pedersen, 1995) that refolded NBD1 and NBD2, or a mixture of the two, hydrolyze ATP with a decreasing enzymatic activity, i.e., NBD1 < NBD2 < NBD1/NBD2. Implementation of this type of information was achieved from studying the effect of the CFTR potentiator molecule, PBF, which previous works indicated that it likely occupies a site located to the interface between NBD1 and NBD2 (Moran et al., 2005; Zegarra-Moran et al., 2007; Melani et al., 2010). We observed that PBF (0-200 uM) does not modify the binding of ATP (calculating the dissociation constant (K_d) by fluorescence spectroscopy) to the dimer, suggesting that indeed ATP and PBF bind to different sites. Conversely, the Michaelis-Menten constant (K_m) for ATP hydrolysis by the dimer increased proportionally to the increase of PBF concentration (see Fig. 2, Paper 2), while the V_{max} value decreased in parallel to the increase in PBF (see Fig. 2, Paper 2) concentration. Given the significance of the constants (Allen, 2008), and in light of the previous finding that the K_d is independent of PBF concentration, we concluded that the action of PBF is essentially due to a decrease in ATP hydrolysis rate. Thus, the decrease of both K_m and V_{max} values likely indicates that the action of PBF is that of a "mixed" inhibitor.

We also found that PBF induced important conformational changes on the NBD1/NBD2 dimer (irrespective to ATP presence), as argued from denaturation experiments (using a given guanidium

concentration) that were carried out with the dimer in the presence, and in the absence, of PBF. We observed that PBF increased the apparent Gibbs free energy difference, ΔG_d, of the transition from the native to the denaturated state, indicating a dimer reduced compactness and an increased accessibility of the denaturant (Pace and Shaw, 2000; Wrabl and Shortle, 1999) after the conformation change, in agreement with the fluorescence quenching produced by potentiator (see Table 1, Paper 2).

However, SAXS experiments were crucial to highlight a dramatic modification of the structural features of the dimer occurring in the presence of both ATP and PBF, whereby R_g significantly increased from 2.11 nm to 3.06 nm, even though the dimer was not disassembled (as indicated by the unaltered mass of the system (see Table 2, Paper 2)). Such an increase of the R_g value is consistent with the increase of the maximum size of the particle, from 6.2 nm (in the presence ATP) to 10.1 nm (adding also PBF), which was estimated from the distance distribution function ($P(r)$) (see Fig. 6b, paper 2). This modification can be explained only by a major conformational change. Accordingly, the $P(r)$ function allowed us to infer that the almost spherical dimer, observed in the sole presence of ATP, became elongated when PBF was added (see also the 3D reconstruction, Fig. 7d, Paper 2).

In agreement with the above-described different accessibility of denaturant, addition of 25 nM PBF produces effects on NBD1/NBD2 dimer that depends on whether ATP is present or not.

In the absence of ATP, NBD1 and NBD2 form a dimer with a molecular mass of about 63 kDa, a value that however gets reduced to about 32 kDa when PBF is added to the dimer. This data is consistent with NBD1 and NBD2 coexisting as monomers, rather that forming a heterodimer: to test this possibility, data were fitted with a weighted sum of the curves shown in Fig. 5b, Paper 2, corresponding to the monomeric NBD1 and NBD2 as measured before (see Paper 1), and the curve

of the putative dimeric conformation shown in Fig. 4, Paper 2. These curves are the reciprocal space fit of scattering computed for the $P(r)$ function calculated for each set of data. Results of the fitting are compatible with the presence of about 3% of the dimer and the remaining being composed by about half of each monomer (Fig. 5, Paper 2), thus we could consider the protein solution as mono-disperse.

In other words, PBF seems to decompose the NBD1/NBD2 dimer, a conclusion that is confirmed from the Kratky plot of the dimer in the presence of PBF (Fig. 7c, Paper 2), showing a globular scattering particle with a double peak, in line with the $P(r)$ function (Fig. 6b, Paper 2) indicating two high-density regions in the complex. (In this case, the presence of two, very similar, independent particles in the system makes it impossible to attempt a three-dimensional reconstruction of the molecules).

Moreover, the presence of 2 mM ATP significantly modifies the effect of 25 nm PBF on the equimolar mixture NBD1/ NBD2. The SAXS spectrum in these conditions, shown in Fig. 6a (Paper 2) is significantly different to that obtained with the potentiator but without ATP (Fig. 5, Paper 2). In this case, the molecular mass estimated from the extrapolation of the intensity to s = 0 is consistent with a dimer, but the dimension of the scattering particle is significantly bigger (Table 2, Paper 2). The gyration radius, R_g, of 2.1 nm measured for the NBD1/NBD2 dimer with ATP increases to 3.1 nm upon addition of 25 nM PBF. This is consistent with about 4 nm increase of the maximum distance, D_{max}, in the distance distribution function. Comparing with $P(r)$ of the NBD1/NBD2 dimer with ATP (Fig. 6b, Paper 2), we can conclude that the potentiator has induced a significant change in the complex. The CFTR-potentiator induces a change in the shape of the NBD1/NBD2 complex, which is compact and about spherical in the presence of ATP, becoming elongated, and with a molecular mass corresponding to that of the two domains.

It is to be noted that our dimer 3D reconstruction, obtained from the SAXS data in the presence of ATP and PBF, does not fit with the crystal structure of isolated NBD1 and NBD2 solved at atomic

resolution. This add an additional proof that PBF changes dramatically the conformation of the dimer in solution.

14 - Structural and biochemical features of RD

A molecular view of RD and an experimental validation of its intrinsic disorder emerge from the combined biophysical and spectroscopic study of RD in the native and phosphorylated states. A control of the identity and the purity of the isolated protein was performed by biochemical techniques (see Fig. 2a, b, Paper 4) while a spectroscopic analysis was performed to verify if the RD was in a folded monomeric state (see Fig. 3a, b, Paper 3).

The bioinformatics analyses also have predicted that RD is an "intrinsically disordered" protein: the probability of disorder (threshold = 0.5) as predicted by the metaPrDOS web server is shown in Fig. 1 of Paper 4, where the disordered regions are indicated by the bars. These disordered regions represent 81% of the sequence (149 out of 185 residues).

Refolded (recombinant) RD was subjected to CD and SAXS studies, before and after the phosphorylation step, to monitor other possible PKA-induced changes. Using the CD technique, we observed that phosphorylation changed dramatically the secondary structure of the protein, whereby a large increase of α-Helix was accompanied by reduction of the β-Sheet and Random Coil contents (see "Results" of Paper 4).

Given its crucial functional importance, in addition to the native (non-phosphorylated) form, we also analyzed the stability of phosphorylated RD. To this end, we followed the ΔG^0 after thermal denaturation (Fig. 2A, Paper 3); specifically, ΔG^0 was evaluated at 10 and 37 °C. Clearly, phosphorylation reduced RD stability, in light of the lower melting point value displayed by phosphorylated RD, and the ΔH between the non-phosphorylated and phosphorylated RD being of

about 6 Kcal/mol. It was hypothesized that activation of CFTR results from the interaction of phosphorylated RD with NBDs (Baker et al., 2007; Ostedgaard et al., 2001). Our data could suggest that phosphorylation induces a conformational change of RD, and/or an increase of the protein flexibility, either of which could favor RD-NBDs interactions.

By SAXS experiments, we then calculated the R_g of both native and phosphorylated RD, whose values (estimated from the Guinier plot) were consistent with non-globular conformations, and in line with the Stoke radius, R_S, value of RD measured from size exclusion chromatography (SEC). From this set of data, we could infer that RD in solution is monomeric, and holds a shape that, however, deviates greatly from that of a typical globular protein.

Accordingly, the observed hydrodynamic behavior (determined by SEC experiments) of both native and phosphorylated RD was intermediate between that of a globular and an unfolded protein (see Fig. 4, Paper 4). Specifically, while the expected R_S value for globular proteins (of molecular mass of 24.3 kDa) is about 2.1 nm, and 4.4 nm for an unfolded protein (Tcherkasskaya et al., 2003), we found a value of 3.6 nm for native RD (only slightly higher than the 3.4 nm value predicted for pre-molten states), and an R_S value of 3.4 nm for phosphorylated RD. This latter value, which is also in the range for a pre-molten proteins, indicated that phosphorylation induces a small reduction of RD size.

These indications, i.e., that phosphorylation changes RD structure, were confirmed by SAXS. The $P(r)$ function shows a maximum that is smaller than $D_{max}/2$ (D_{max} is the maximum particle diameter) (Fig. 6, Paper 4), corresponding to elongated molecules (Feigin and Svergun, 1987; Svergun and Koch, 2002). Consistently, the *ab initio* molecular shape reconstructed from the SAXS data resulted in elongated molecules for both native and phosphorylated RD (see Fig. 8, Paper 4).

Also Ensemble Optimization Method (EOM) analyses indicated differences between the ensembles for the native and phosphorylated RD, essentially that phosphorylated RD had a smaller average R_g and D_{max} than the native protein. (Fig. 7b, c, Paper 4). The best EOM ensembles, which account for the continuous light-gray lines in Fig. 5 of Paper 4, are composed by 16 and 19 structures for the native and phosphorylated RD. The average anisometry (Bernadò et al., 2007) evaluated for all the EOM ensemble models was 2.1 ± 0.6 and 1.7 ± 0.3 nm, for the native and the phosphorylated RD, respectively, indicating that the molecules have a prolate shape, being the phosphorylated RD more compact.

The main conclusions that one can draw from the data regarding the structural features of the intracellular domains of CFTR are the following:

- NBD1 and NBD2 dimerize spontaneously when present in isomolar concentration.
- The binding of ATP induces a conformational change rendering the dimer tighter.
- The CFTR potentiator, PBF, modifies the enzymatic activity of the NBD1/NBD2dimer. However, reconstruction of the dimer *ab initio* model indicates that PBF also changes the dimer conformation.
- Phosphorylation of RD diminishes the protein stability and induces a significant change of the percentage of the contributing secondary structures.
- For the first time, an experimentally-based model for RD was provided by SAXS experiments.

It is therefore possible that, together with the provided low-resolution models and those that eventually will derive from CF-related NBD mutants, the here-presented biochemical and biophysical characterization of the intracellular CFTR domains may have future implications in further our understanding of the pathophysiology of CFTR.

Bibliography

1. Correlation between genotype and phenotype in patients with cystic fibrosis. The Cystic Fibrosis Genotype-Phenotype Consortium. N Engl J Med 329: 1308-13, 1993.

2. Adams PD, Chen Y, Ma K, Zagorski MG, Sonnichsen FD, McLaughlin ML and Barkley MD: Intramolecular quenching of tryptophan fluorescence by the peptide bond in cyclic hexapeptides. J Am Chem Soc 124: 9278-86, 2002.

3. Ai T, Bompadre SG, Wang X, Hu S, Li M and Hwang TC: Capsaicin potentiates wild-type and mutant cystic fibrosis transmembrane conductance regulator chloride-channel currents. Mol Pharmacol 65: 1415-26, 2004.

4. Aleksandrov L, Mengos A, Chang X, Aleksandrov A and Riordan JR: Differential interactions of nucleotides at the two nucleotide binding domains of the cystic fibrosis transmembrane conductance regulator. J Biol Chem 276: 12918-23, 2001.

5. Al-Nakkash L, Hu S, Li M and Hwang TC: A common mechanism for cystic fibrosis transmembrane conductance regulator protein activation by genistein and benzimidazolone analogs. J Pharmacol Exp Ther 296: 464-72, 2001.

6. Augarten A, Hacham S, Kerem E, Sheva Kerem B, Szeinberg A, Laufer J, Doolman R, Altshuler R, Blau H, Bentur L and et al.: The significance of sweat Cl/Na ratio in patients with borderline sweat test. Pediatr Pulmonol 20: 369-71, 1995.

7. Awayn NH, Rosenberg MF, Kamis AB, Aleksandrov LA, Riordan JR and Ford RC: Crystallographic and single-particle analyses of native- and nucleotide-bound forms of the cystic fibrosis transmembrane conductance regulator (CFTR) protein. Biochem Soc Trans 33: 996-9, 2005.

8. Baker JM, Hudson RP, Kanelis V, Choy WY, Thibodeau PH, Thomas PJ and Forman-Kay JD: CFTR regulatory region interacts with NBD1 predominantly via multiple transient helices. Nat Struct Mol Biol 14: 738-45, 2007.

9. Barkley MD, Chen Q, Walczak WJ and Maskos K: Time-resolved fluorescence studies of tomaymycin bonding to synthetic DNAs. Biophys J 70: 1923-32, 1996.

10. Baroni D, Zegarra-Moran O, Svensson A and Moran O: Direct interaction of a CFTR potentiator and a CFTR corrector with phospholipid bilayers. Eur Biophys J 43: 341-6, 2014.

11. Becq F, Mall MA, Sheppard DN, Conese M and Zegarra-Moran O: Pharmacological therapy for cystic fibrosis: from bench to bedside. J Cyst Fibros 10 Suppl 2: S129-45, 2011.

12. Bent DV and Hayon E: Excited state chemistry of aromatic amino acids and related peptides. III. Tryptophan. J Am Chem Soc 97: 2612-9, 1975.

13. Bernado P, Mylonas E, Petoukhov MV, Blackledge M and Svergun DI: Structural characterization of flexible proteins using small-angle X-ray scattering. J Am Chem Soc 129: 5656-64, 2007.

14. Blackman SM, Deering-Brose R, McWilliams R, Naughton K, Coleman B, Lai T, Algire M, Beck S, Hoover-Fong J, Hamosh A, Fallin MD, West K, Arking DE, Chakravarti A, Cutler DJ and Cutting GR: Relative contribution of genetic and nongenetic modifiers to intestinal obstruction in cystic fibrosis. Gastroenterology 131: 1030-9, 2006.

15. Bondos SE and Bicknell A: Detection and prevention of protein aggregation before, during, and after purification. Anal Biochem 316: 223-31, 2003.

16. Bonfield TL, Konstan MW and Berger M: Altered respiratory epithelial cell cytokine production in cystic fibrosis. J Allergy Clin Immunol 104: 72-8, 1999.

17. Boucher RC: Human airway ion transport. Part two. Am J Respir Crit Care Med 150: 581-93, 1994.

18. Boucher RC: Molecular insights into the physiology of the 'thin film' of airway surface liquid. J Physiol 516 (Pt 3): 631-8, 1999.

19. Boucher RC: Airway surface dehydration in cystic fibrosis: pathogenesis and therapy. Annu Rev Med 58: 157-70, 2007.

20. Boucher RC: Cystic fibrosis: a disease of vulnerability to airway surface dehydration. Trends Mol Med 13: 231-40, 2007.

21. Boyle MP: Nonclassic cystic fibrosis and CFTR-related diseases. Curr Opin Pulm Med 9: 498-503, 2003.

22. Caci E, Folli C, Zegarra-Moran O, Ma T, Springsteel MF, Sammelson RE, Nantz MH, Kurth MJ, Verkman AS and Galietta LJ: CFTR activation in human bronchial epithelial cells by novel benzoflavone and benzimidazolone compounds. Am J Physiol Lung Cell Mol Physiol 285: L180-8, 2003.

23. Callis PR: 1La and 1Lb transitions of tryptophan: applications of theory and experimental observations to fluorescence of proteins. Methods Enzymol 278: 113-50, 1997.

24. Campbell PW, 3rd, Parker RA, Roberts BT, Krishnamani MR and Phillips JA, 3rd: Association of poor clinical status and heavy exposure to tobacco smoke in patients with cystic fibrosis who are homozygous for the F508 deletion. J Pediatr 120: 261-4, 1992.

25. Campodonico VL, Gadjeva M, Paradis-Bleau C, Uluer A and Pier GB: Airway epithelial control of Pseudomonas aeruginosa infection in cystic fibrosis. Trends Mol Med 14: 120-33, 2008.

26. Carlstedt-Duke J, Bronnegard M and Strandvik B: Pathological regulation of arachidonic acid release in cystic fibrosis: the putative basic defect. Proc Natl Acad Sci U S A 83: 9202-6, 1986.

27. Carrabino S, Carpani D, Livraghi A, Di Cicco M, Costantini D, Copreni E, Colombo C and Conese M: Dysregulated interleukin-8 secretion and NF-kappaB activity in human cystic fibrosis nasal epithelial cells. J Cyst Fibros 5: 113-9, 2006.

28. Castellani C, Cuppens H, Macek M, Jr., Cassiman JJ, Kerem E, Durie P, Tullis E, Assael BM, Bombieri C, Brown A, Casals T, Claustres M, Cutting GR, Dequeker E, Dodge J, Doull I, Farrell P, Ferec C, Girodon E, Johannesson M, Kerem B, Knowles M, Munck A, Pignatti PF, Radojkovic D, Rizzotti P, Schwarz M, Stuhrmann M, Tzetis M, Zielenski J and Elborn JS: Consensus on the use and interpretation of cystic fibrosis mutation analysis in clinical practice. J Cyst Fibros 7: 179-96, 2008.

29. Chacon P, Moran F, Diaz JF, Pantos E and Andreu JM: Low-resolution structures of proteins in solution retrieved from X-ray scattering with a genetic algorithm. Biophys J 74: 2760-75, 1998.

30. Chambers LA, Rollins BM and Tarran R: Liquid movement across the surface epithelium of large airways. Respir Physiol Neurobiol 159: 256-70, 2007.

31. Chang XB, Tabcharani JA, Hou YX, Jensen TJ, Kartner N, Alon N, Hanrahan JW and Riordan JR: Protein kinase A (PKA) still activates CFTR chloride channel after mutagenesis of all 10 PKA consensus phosphorylation sites. J Biol Chem 268: 11304-11, 1993.

32. Chappe V, Irvine T, Liao J, Evagelidis A and Hanrahan JW: Phosphorylation of CFTR by PKA promotes binding of the regulatory domain. EMBO J 24: 2730-40, 2005.

33. Chen Y and Barkley MD: Toward understanding tryptophan fluorescence in proteins. Biochemistry 37: 9976-82, 1998.

34. Collaco JM, Vanscoy L, Bremer L, McDougal K, Blackman SM, Bowers A, Naughton K, Jennings J, Ellen J and Cutting GR: Interactions between secondhand smoke and genes that affect cystic fibrosis lung disease. JAMA 299: 417-24, 2008.

35. Cortijo M, Llor J and Sanchez-Ruiz JM: Thermodynamic constants for tautomerism, hydration, and ionization of vitamin B6 compounds in water/dioxane. J Biol Chem 263: 17960-9, 1988.

36. Costerton JW, Stewart PS and Greenberg EP: Bacterial biofilms: a common cause of persistent infections. Science 284: 1318-22, 1999.

37. Csanady L, Chan KW, Seto-Young D, Kopsco DC, Nairn AC and Gadsby DC: Severed channels probe regulation of gating of cystic fibrosis transmembrane conductance regulator by its cytoplasmic domains. J Gen Physiol 116: 477-500, 2000.

38. Csanady L, Seto-Young D, Chan KW, Cenciarelli C, Angel BB, Qin J, McLachlin DT, Krutchinsky AN, Chait BT, Nairn AC and Gadsby DC: Preferential phosphorylation of R-domain Serine 768 dampens activation of CFTR channels by PKA. J Gen Physiol 125: 171-86, 2005.

39. Cui L, Aleksandrov L, Chang XB, Hou YX, He L, Hegedus T, Gentzsch M, Aleksandrov A, Balch WE and Riordan JR: Domain interdependence in the biosynthetic assembly of CFTR. J Mol Biol 365: 981-94, 2007.

40. De Boeck K, Wilschanski M, Castellani C, Taylor C, Cuppens H, Dodge J and Sinaasappel M: Cystic fibrosis: terminology and diagnostic algorithms. Thorax 61: 627-35, 2006.

41. de Gracia J, Mata F, Alvarez A, Casals T, Gatner S, Vendrell M, de la Rosa D, Guarner L and Hermosilla E: Genotype-phenotype correlation for pulmonary function in cystic fibrosis. Thorax 60: 558-63, 2005.

42. Dorfman R, Sandford A, Taylor C, Huang B, Frangolias D, Wang Y, Sang R, Pereira L, Sun L, Berthiaume Y, Tsui LC, Pare PD, Durie P, Corey M and Zielenski J: Complex two-gene modulation of lung disease severity in children with cystic fibrosis. J Clin Invest 118: 1040-9, 2008.

43. Drumm ML, Konstan MW, Schluchter MD, Handler A, Pace R, Zou F, Zariwala M, Fargo D, Xu A, Dunn JM, Darrah RJ, Dorfman R, Sandford AJ, Corey M, Zielenski J, Durie P, Goddard K, Yankaskas JR, Wright FA and Knowles MR: Genetic modifiers of lung disease in cystic fibrosis. N Engl J Med 353: 1443-53, 2005.

44. Dulhanty AM, Chang XB and Riordan JR: Mutation of potential phosphorylation sites in the recombinant R domain of the cystic fibrosis transmembrane conductance regulator has significant effects on domain conformation. Biochem Biophys Res Commun 206: 207-14, 1995.

45. Eftink MR: Fluorescence techniques for studying protein structure. Methods Biochem Anal 35: 127-205, 1991.

46. Fanen P, Wohlhuter-Haddad A and Hinzpeter A: Genetics of cystic fibrosis: CFTR mutation classifications toward genotype-based CF therapies. Int J Biochem Cell Biol 52: 94-102, 2014.

47. Feigin L and Svergun D: Structure analysis by small-angle X-ray and neutron scattering. . In: Plenum Press, New York, 1987.

48. Franke D and Svergun DI: DAMMIF, a program for rapid ab-initio shape determination in small-angle scattering J. Appl. Cryst. 42: 342-346, 2009.

49. Freedman SD, Blanco PG, Zaman MM, Shea JC, Ollero M, Hopper IK, Weed DA, Gelrud A, Regan MM, Laposata M, Alvarez JG and O'Sullivan BP: Association of cystic fibrosis with abnormalities in fatty acid metabolism. N Engl J Med 350: 560-9, 2004.

50. Gadsby DC, Vergani P and Csanady L: The ABC protein turned chloride channel whose failure causes cystic fibrosis. Nature 440: 477-83, 2006.

51. Galietta LV, Jayaraman S and Verkman AS: Cell-based assay for high-throughput quantitative screening of CFTR chloride transport agonists. Am J Physiol Cell Physiol 281: C1734-42, 2001.

52. Gilljam H, Ellin A and Strandvik B: Increased bronchial chloride concentration in cystic fibrosis. Scand J Clin Lab Invest 49: 121-4, 1989.

53. Glatter O: A new method for the evaluation of small-angle scattering data. 10: 415-421., 1977.

54. Glatter O and Kratky O: Porod General theory. Small-angle X-ray scattering,. In: 1982, pp 17-51.

55. Guinier A and Fournet G: Small-angle scattering of X-rays. In: Wiley, New York, 1955.

56. Haardt M, Benharouga M, Lechardeur D, Kartner N and Lukacs GL: C-terminal truncations destabilize the cystic fibrosis transmembrane conductance regulator without impairing its biogenesis. A novel class of mutation. J Biol Chem 274: 21873-7, 1999.

57. Hegedus T, Aleksandrov A, Cui L, Gentzsch M, Chang XB and Riordan JR: F508del CFTR with two altered RXR motifs escapes from ER quality control but its channel activity is thermally sensitive. Biochim Biophys Acta 1758: 565-72, 2006.

58. Highsmith WE, Burch LH, Zhou Z, Olsen JC, Boat TE, Spock A, Gorvoy JD, Quittel L, Friedman KJ, Silverman LM and et al.: A novel mutation in the cystic fibrosis gene in patients with pulmonary disease but normal sweat chloride concentrations. N Engl J Med 331: 974-80, 1994.

59. Imundo L, Barasch J, Prince A and Al-Awqati Q: Cystic fibrosis epithelial cells have a receptor for pathogenic bacteria on their apical surface. Proc Natl Acad Sci U S A 92: 3019-23, 1995.

60. Jayaraman S, Haggie P, Wachter RM, Remington SJ and Verkman AS: Mechanism and cellular applications of a green fluorescent protein-based halide sensor. J Biol Chem 275: 6047-50, 2000.

61. Kalid O, Mense M, Fischman S, Shitrit A, Bihler H, Ben-Zeev E, Schutz N, Pedemonte N, Thomas PJ, Bridges RJ, Wetmore DR, Marantz Y and Senderowitz H: Small molecule correctors of F508del-CFTR discovered by structure-based virtual screening. J Comput Aided Mol Des 24: 971-91, 2010.

62. Kanelis V, Hudson RP, Thibodeau PH, Thomas PJ and Forman-Kay JD: NMR evidence for differential phosphorylation-dependent interactions in WT and DeltaF508 CFTR. EMBO J 29: 263-77, 2010.

63. Karp CL, Flick LM, Park KW, Softic S, Greer TM, Keledjian R, Yang R, Uddin J, Guggino WB, Atabani SF, Belkaid Y, Xu Y, Whitsett JA, Accurso FJ, Wills-Karp M and Petasis NA: Defective lipoxin-mediated anti-inflammatory activity in the cystic fibrosis airway. Nat Immunol 5: 388-92, 2004.

64. Karpowich N, Martsinkevich O, Millen L, Yuan YR, Dai PL, MacVey K, Thomas PJ and Hunt JF: Crystal structures of the MJ1267 ATP binding cassette reveal an induced-fit effect at the ATPase active site of an ABC transporter. Structure 9: 571-86, 2001.

65. Khan TZ, Wagener JS, Bost T, Martinez J, Accurso FJ and Riches DW: Early pulmonary inflammation in infants with cystic fibrosis. Am J Respir Crit Care Med 151: 1075-82, 1995.

66. Kidd JF, Ramjeesingh M, Stratford F, Huan LJ and Bear CE: A heteromeric complex of the two nucleotide binding domains of cystic fibrosis transmembrane conductance regulator (CFTR) mediates ATPase activity. J Biol Chem 279: 41664-9, 2004.

67. Knowles MR and Boucher RC: Mucus clearance as a primary innate defense mechanism for mammalian airways. J Clin Invest 109: 571-7, 2002.

68. Ko YH and Pedersen PL: The first nucleotide binding fold of the cystic fibrosis transmembrane conductance regulator can function as an active ATPase. J Biol Chem 270: 22093-6, 1995.

69. Koch MH, Vachette P and Svergun DI: Small-angle scattering: a view on the properties, structures and structural changes of biological macromolecules in solution. Q Rev Biophys 36: 147-227, 2003.

70. Konig S, Svergun DI, Volkov VV, Feigin LA and Koch MH: Small-angle X-ray solution-scattering studies on ligand-induced subunit interactions of the thiamine diphosphate dependent enzyme pyruvate decarboxylase from different organisms. Biochemistry 37: 5329-34, 1998.

71. Kozin M and Svergun D: Automated matching of high- and low-resolution structural models. J. Appl. Cryst. 34: 33-41, 20014.

72. Kreda SM, Davis CW and Rose MC: CFTR, mucins, and mucus obstruction in cystic fibrosis. Cold Spring Harb Perspect Med 2: a009589, 2012.

73. Lao O, Andres AM, Mateu E, Bertranpetit J and Calafell F: Spatial patterns of cystic fibrosis mutation spectra in European populations. Eur J Hum Genet 11: 385-94, 2003.

74. Lazarowski ER and Boucher RC: UTP as an extracellular signaling molecule. News Physiol Sci 16: 1-5, 2001.

75. LeGrys VA: Sweat testing for the diagnosis of cystic fibrosis: practical considerations. J Pediatr 129: 892-7, 1996.

76. LeGrys VA: Assessment of sweat-testing practices for the diagnosis of cystic fibrosis. Arch Pathol Lab Med 125: 1420-4, 2001.

77. Lewis HA, Buchanan SG, Burley SK, Conners K, Dickey M, Dorwart M, Fowler R, Gao X, Guggino WB, Hendrickson WA, Hunt JF, Kearins MC, Lorimer D, Maloney PC, Post KW, Rajashankar KR, Rutter ME, Sauder JM, Shriver S, Thibodeau PH, Thomas PJ, Zhang M, Zhao X and Emtage S: Structure of nucleotide-binding domain 1 of the cystic fibrosis transmembrane conductance regulator. EMBO J 23: 282-93, 2004.

78. Lewis HA, Zhao X, Wang C, Sauder JM, Rooney I, Noland BW, Lorimer D, Kearins MC, Conners K, Condon B, Maloney PC, Guggino WB, Hunt JF and Emtage S: Impact of the deltaF508 mutation in first nucleotide-binding domain of human cystic fibrosis transmembrane conductance regulator on domain folding and structure. J Biol Chem 280: 1346-53, 2005.

79. Linsdell P: Cystic fibrosis transmembrane conductance regulator chloride channel blockers: Pharmacological, biophysical and physiological relevance. World J Biol Chem 5: 26-39, 2014.

80. Logan J, Hiestand D, Daram P, Huang Z, Muccio DD, Hartman J, Haley B, Cook WJ and Sorscher EJ: Cystic fibrosis transmembrane conductance regulator mutations that disrupt nucleotide binding. J Clin Invest 94: 228-36, 1994.

81. Lu NT and Pedersen PL: Cystic fibrosis transmembrane conductance regulator: the purified NBF1+R protein interacts with the purified NBF2 domain to form a stable NBF1+R/NBF2 complex while inducing a conformational change transmitted to the C-terminal region. Arch Biochem Biophys 375: 7-20, 2000.

82. Ma J, Zhao J, Drumm ML, Xie J and Davis PB: Function of the R domain in the cystic fibrosis transmembrane conductance regulator chloride channel. J Biol Chem 272: 28133-41, 1997.

83. MacDonald KD, McKenzie KR and Zeitlin PL: Cystic fibrosis transmembrane regulator protein mutations: 'class' opportunity for novel drug innovation. Paediatr Drugs 9: 1-10, 2007.

84. Matsui H, Davis CW, Tarran R and Boucher RC: Osmotic water permeabilities of cultured, well-differentiated normal and cystic fibrosis airway epithelia. J Clin Invest 105: 1419-27, 2000.

85. Matsui H, Grubb BR, Tarran R, Randell SH, Gatzy JT, Davis CW and Boucher RC: Evidence for periciliary liquid layer depletion, not abnormal ion composition, in the pathogenesis of cystic fibrosis airways disease. Cell 95: 1005-15, 1998.

86. Matsui H, Wagner VE, Hill DB, Schwab UE, Rogers TD, Button B, Taylor RM, 2nd, Superfine R, Rubinstein M, Iglewski BH and Boucher RC: A physical linkage between cystic fibrosis airway surface dehydration and Pseudomonas aeruginosa biofilms. Proc Natl Acad Sci U S A 103: 18131-6, 2006.

87. Melani R, Tomati V, Galietta LJ and Zegarra-Moran O: Modulation of cystic fibrosis transmembrane conductance regulator (CFTR) activity and genistein binding by cytosolic pH. J Biol Chem 285: 41591-6, 2010.

88. Mense M, Vergani P, White DM, Altberg G, Nairn AC and Gadsby DC: In vivo phosphorylation of CFTR promotes formation of a nucleotide-binding domain heterodimer. EMBO J 25: 4728-39, 2006.

89. Mertens HD and Svergun DI: Structural characterization of proteins and complexes using small-angle X-ray solution scattering. J Struct Biol 172: 128-41, 2010.

90. Mishra A, Greaves R and Massie J: The relevance of sweat testing for the diagnosis of cystic fibrosis in the genomic era. Clin Biochem Rev 26: 135-53, 2005.

91. Moran O: Model of the cAMP activation of chloride transport by CFTR channel and the mechanism of potentiators. J Theor Biol 262: 73-9, 2010.

92. Moran O: On the structural organization of the intracellular domains of CFTR. Int J Biochem Cell Biol 52: 7-14, 2014.

93. Moran O, Galietta LJ and Zegarra-Moran O: Binding site of activators of the cystic fibrosis transmembrane conductance regulator in the nucleotide binding domains. Cell Mol Life Sci 62: 446-60, 2005.

94. Moran O and Zegarra-Moran O: On the measurement of the functional properties of the CFTR. J Cyst Fibros 7: 483-94, 2008.

95. Mornon JP, Lehn P and Callebaut I: Molecular models of the open and closed states of the whole human CFTR protein. Cell Mol Life Sci 66: 3469-86, 2009.

96. Mylonas E and Svergun DI: Accuracy of molecular mass determination of proteins in solution by small-angle X-ray scattering. . J. Appl. Cryst. 40: s245-s249, 2007.

97. Neville DC, Rozanas CR, Price EM, Gruis DB, Verkman AS and Townsend RR: Evidence for phosphorylation of serine 753 in CFTR using a novel metal-ion affinity resin and matrix-assisted laser desorption mass spectrometry. Protein Sci 6: 2436-45, 1997.

98. Ostedgaard LS, Baldursson O and Welsh MJ: Regulation of the cystic fibrosis transmembrane conductance regulator Cl- channel by its R domain. J Biol Chem 276: 7689-92, 2001.

99. O'Sullivan BP and Freedman SD: Cystic fibrosis. Lancet 373: 1891-904, 2009.

100. O'Sullivan BP and Michelson AD: The inflammatory role of platelets in cystic fibrosis. Am J Respir Crit Care Med 173: 483-90, 2006.

101. Pace CN and Shaw KL: Linear extrapolation method of analyzing solvent denaturation curves. Proteins Suppl 4: 1-7, 2000.

102. Pedemonte N, Sonawane ND, Taddei A, Hu J, Zegarra-Moran O, Suen YF, Robins LI, Dicus CW, Willenbring D, Nantz MH, Kurth MJ, Galietta LJ and Verkman AS: Phenylglycine and sulfonamide correctors of defective delta F508 and G551D cystic fibrosis transmembrane conductance regulator chloride-channel gating. Mol Pharmacol 67: 1797-807, 2005.

103. Pedemonte N, Zegarra-Moran O and Galietta LJ: High-throughput screening of libraries of compounds to identify CFTR modulators. Methods Mol Biol 741: 13-21, 2011.

104. Petoukhov MV, Franke D, Shkumatov AV, Tria G, Kikhney AG, Gajda M, Gorba C, Mertens HDT, Konarev PV and Svergun DI: New developments in the ATSAS program package for small-angle scattering data analysis. Â© International Union of Crystallography. J. Appl. Cryst. 45: 342-350 2012.

105. Petoukhov MV and Svergun DI: Applications of small-angle X-ray scattering to biomacromolecular solutions. Int J Biochem Cell Biol 45: 429-37, 2013.

106. Pranke IM and Sermet-Gaudelus I: Biosynthesis of cystic fibrosis transmembrane conductance regulator. Int J Biochem Cell Biol 52: 26-38, 2014.

107. Qu BH, Strickland EH and Thomas PJ: Localization and suppression of a kinetic defect in cystic fibrosis transmembrane conductance regulator folding. J Biol Chem 272: 15739-44, 1997.

108. Quillin ML and Matthews BW: Accurate calculation of the density of proteins. Acta Crystallogr D Biol Crystallogr 56: 791-4, 2000.

109. Quinton PM: Physiological basis of cystic fibrosis: a historical perspective. Physiol Rev 79: S3-S22, 1999.

110. Ramsey BW, Davies J, McElvaney NG, Tullis E, Bell SC, Drevinek P, Griese M, McKone EF, Wainwright CE, Konstan MW, Moss R, Ratjen F, Sermet-Gaudelus I, Rowe SM, Dong Q, Rodriguez S, Yen K, Ordonez C and Elborn JS: A CFTR potentiator in patients with cystic fibrosis and the G551D mutation. N Engl J Med 365: 1663-72, 2011.

111. Randell SH and Boucher RC: Effective mucus clearance is essential for respiratory health. Am J Respir Cell Mol Biol 35: 20-8, 2006.

112. Raviv U, Giasson S, Kampf N, Gohy JF, Jerome R and Klein J: Lubrication by charged polymers. Nature 425: 163-5, 2003.

113. Reisin IL, Prat AG, Abraham EH, Amara JF, Gregory RJ, Ausiello DA and Cantiello HF: The cystic fibrosis transmembrane conductance regulator is a dual ATP and chloride channel. J Biol Chem 269: 20584-91, 1994.

114. Rich DP, Gregory RJ, Anderson MP, Manavalan P, Smith AE and Welsh MJ: Effect of deleting the R domain on CFTR-generated chloride channels. Science 253: 205-7, 1991.

115. Riordan JR: CFTR function and prospects for therapy. Annu Rev Biochem 77: 701-26, 2008.

116. Riordan JR, Rommens JM, Kerem B, Alon N, Rozmahel R, Grzelczak Z, Zielenski J, Lok S, Plavsic N, Chou JL and et al.: Identification of the cystic fibrosis gene: cloning and characterization of complementary DNA. Science 245: 1066-73, 1989.

117. Rogan MP, Stoltz DA and Hornick DB: Cystic fibrosis transmembrane conductance regulator intracellular processing, trafficking, and opportunities for mutation-specific treatment. Chest 139: 1480-90, 2011.

118. Rose MC and Voynow JA: Respiratory tract mucin genes and mucin glycoproteins in health and disease. Physiol Rev 86: 245-78, 2006.

119. Rosenberg MF, Callaghan R, Modok S, Higgins CF and Ford RC: Three-dimensional structure of P-glycoprotein: the transmembrane regions adopt an asymmetric configuration in the nucleotide-bound state. J Biol Chem 280: 2857-62, 2005.

120. Rosenberg MF, O'Ryan LP, Hughes G, Zhao Z, Aleksandrov LA, Riordan JR and Ford RC: The cystic fibrosis transmembrane conductance regulator (CFTR): three-dimensional structure and localization of a channel gate. J Biol Chem 286: 42647-54, 2011.

121. Rosenstein BJ: Nonclassic cystic fibrosis: a clinical conundrum. Pediatr Pulmonol 36: 10-2, 2003.

122. Roth EK, Hirtz S, Duerr J, Wenning D, Eichler I, Seydewitz HH, Amaral MD and Mall MA: The K+ channel opener 1-EBIO potentiates residual function of mutant CFTR in rectal biopsies from cystic fibrosis patients. PLoS One 6: e24445, 2011.

123. Rottner M, Kunzelmann C, Mergey M, Freyssinet JM and Martinez MC: Exaggerated apoptosis and NF-kappaB activation in pancreatic and tracheal cystic fibrosis cells. FASEB J 21: 2939-48, 2007.

124. Sanchez-Ruiz JM, Lopez-Lacomba JL, Cortijo M and Mateo PL: Differential scanning calorimetry of the irreversible thermal denaturation of thermolysin. Biochemistry 27: 1648-52, 1988.

125. Sanchez-Ruiz JM and Martinez-Carrion M: A Fourier-transform infrared spectroscopic study of the phosphoserine residues in hen egg phosvitin and ovalbumin. Biochemistry 27: 3338-42, 1988.

126. Schwiebert EM, Egan ME, Hwang TH, Fulmer SB, Allen SS, Cutting GR and Guggino WB: CFTR regulates outwardly rectifying chloride channels through an autocrine mechanism involving ATP. Cell 81: 1063-73, 1995.

127. Seibert FS, Tabcharani JA, Chang XB, Dulhanty AM, Mathews C, Hanrahan JW and Riordan JR: cAMP-dependent protein kinase-mediated phosphorylation of cystic fibrosis transmembrane conductance regulator residue Ser-753 and its role in channel activation. J Biol Chem 270: 2158-62, 1995.

128. Smith JJ, Travis SM, Greenberg EP and Welsh MJ: Cystic fibrosis airway epithelia fail to kill bacteria because of abnormal airway surface fluid. Cell 85: 229-36, 1996.

129. Sreerama N and Woody RW: Computation and analysis of protein circular dichroism spectra. Methods Enzymol 383: 318-51, 2004.

130. Strandvik B, Bjorck E, Fallstrom M, Gronowitz E, Thountzouris J, Lindblad A, Markiewicz D, Wahlstrom J, Tsui LC and Zielenski J: Spectrum of mutations in the CFTR gene of patients with classical and atypical forms of cystic fibrosis from southwestern Sweden: identification of 12 novel mutations. Genet Test 5: 235-42, 2001.

131. Stutts MJ, Canessa CM, Olsen JC, Hamrick M, Cohn JA, Rossier BC and Boucher RC: CFTR as a cAMP-dependent regulator of sodium channels. Science 269: 847-50, 1995.

132. Svergun D and Koch M: Advances in structure analysis using small-angle scattering in solution. Curr. Opin. Struct. Biol. 12: 654-660, 2002.

133. Svergun DI: Determination of the regularization parameter in indirect-transform methods using perceptual criteria. J. Appl. Crystallogr. 25: 495-503., 1992.

134. Svergun DI: Restoring low resolution structure of biological macromolecules from solution scattering using simulated annealing. Biophys J 76: 2879-86, 1999.

135. Svergun DI and Koch MH: Advances in structure analysis using small-angle scattering in solution. Curr Opin Struct Biol 12: 654-60, 2002.

136. Svergun DI, Petoukhov MV and Koch MH: Determination of domain structure of proteins from X-ray solution scattering. Biophys J 80: 2946-53, 2001.

137. Tcherkasskaya O, Davidson EA and Uversky VN: Biophysical constraints for protein structure prediction. J Proteome Res 2: 37-42, 2003.

138. Tello-Solis SR and Hernandez-Arana A: Effect of irreversibility on the thermodynamic characterization of the thermal denaturation of Aspergillus saitoi acid proteinase. Biochem J 311 (Pt 3): 969-74, 1995.

139. Tello-Solis SR and Romero-Garcia B: Thermal denaturation of porcine pepsin: a study by circular dichroism. Int J Biol Macromol 28: 129-33, 2001.

140. Thibodeau PH, Brautigam CA, Machius M and Thomas PJ: Side chain and backbone contributions of Phe508 to CFTR folding. Nat Struct Mol Biol 12: 10-6, 2005.

141. Tirouvanziam R, de Bentzmann S, Hubeau C, Hinnrasky J, Jacquot J, Peault B and Puchelle E: Inflammation and infection in naive human cystic fibrosis airway grafts. Am J Respir Cell Mol Biol 23: 121-7, 2000.

142. Townsend RR, Lipniunas PH, Tulk BM and Verkman AS: Identification of protein kinase A phosphorylation sites on NBD1 and R domains of CFTR using electrospray mass spectrometry with selective phosphate ion monitoring. Protein Sci 5: 1865-73, 1996.

143. Tsai J, Taylor R, Chothia C and Gerstein M: The packing density in proteins: standard radii and volumes. J Mol Biol 290: 253-66, 1999.

144. Vais H, Zhang R and Reenstra WW: Dibasic phosphorylation sites in the R domain of CFTR have stimulatory and inhibitory effects on channel activation. Am J Physiol Cell Physiol 287: C737-45, 2004.

145. Van Goor F, Hadida S, Grootenhuis PD, Burton B, Stack JH, Straley KS, Decker CJ, Miller M, McCartney J, Olson ER, Wine JJ, Frizzell RA, Ashlock M and Negulescu PA: Correction of the F508del-CFTR protein processing defect in vitro by the investigational drug VX-809. Proc Natl Acad Sci U S A 108: 18843-8, 2011.

146. Van Goor F, Straley KS, Cao D, Gonzalez J, Hadida S, Hazlewood A, Joubran J, Knapp T, Makings LR, Miller M, Neuberger T, Olson E, Panchenko V, Rader J, Singh A, Stack JH, Tung R, Grootenhuis PD and Negulescu P: Rescue of DeltaF508-CFTR trafficking and gating in human cystic fibrosis airway primary cultures by small molecules. Am J Physiol Lung Cell Mol Physiol 290: L1117-30, 2006.

147. Vankeerberghen A, Cuppens H and Cassiman JJ: The cystic fibrosis transmembrane conductance regulator: an intriguing protein with pleiotropic functions. J Cyst Fibros 1: 13-29, 2002.

148. Vergani P, Lockless SW, Nairn AC and Gadsby DC: CFTR channel opening by ATP-driven tight dimerization of its nucleotide-binding domains. Nature 433: 876-80, 2005.

149. Volkov VV and Svergun DI: Uniqueness of ab-initio shape determination in small-angle scattering. J. Appl. Cryst. 36: 860-864.

150. Welsh MJ and Ramsey BW: Research on cystic fibrosis: a journey from the Heart House. Am J Respir Crit Care Med 157: S148-54, 1998.

151. Welsh MJ and Smith AE: Molecular mechanisms of CFTR chloride channel dysfunction in cystic fibrosis. Cell 73: 1251-4, 1993.

152. Welsh MJ and Smith JJ: cAMP stimulation of HCO3- secretion across airway epithelia. JOP 2: 291-3, 2001.

153. Whitmore L and Wallace BA: Protein secondary structure analyses from circular dichroism spectroscopy: methods and reference databases. Biopolymers 89: 392-400, 2008.

154. Wilkinson DJ, Strong TV, Mansoura MK, Wood DL, Smith SS, Collins FS and Dawson DC: CFTR activation: additive effects of stimulatory and inhibitory phosphorylation sites in the R domain. Am J Physiol 273: L127-33, 1997.

155. Worlitzsch D, Tarran R, Ulrich M, Schwab U, Cekici A, Meyer KC, Birrer P, Bellon G, Berger J, Weiss T, Botzenhart K, Yankaskas JR, Randell S, Boucher RC and Doring G: Effects of reduced mucus oxygen concentration in airway Pseudomonas infections of cystic fibrosis patients. J Clin Invest 109: 317-25, 2002.

156. Wrabl J and Shortle D: A model of the changes in denatured state structure underlying m value effects in staphylococcal nuclease. Nat Struct Biol 6: 876-83, 1999.

157. Wriggers W: Using Situs for the integration of multi-resolution structures. Biophys Rev 2: 21-27, 2010.

158. Wriggers W and Chacon P: Modeling tricks and fitting techniques for multiresolution structures. Structure 9: 779-88, 2001.

159. Zabner J, Smith JJ, Karp PH, Widdicombe JH and Welsh MJ: Loss of CFTR chloride channels alters salt absorption by cystic fibrosis airway epithelia in vitro. Mol Cell 2: 397-403, 1998.

160. Zegarra-Moran O, Monteverde M, Galietta LJ and Moran O: Functional analysis of mutations in the putative binding site for cystic fibrosis transmembrane conductance regulator potentiators. Interaction between activation and inhibition. J Biol Chem 282: 9098-104, 2007.

161. Zhang L, Aleksandrov LA, Riordan JR and Ford RC: Domain location within the cystic fibrosis transmembrane conductance regulator protein investigated by electron microscopy and gold labelling. Biochim Biophys Acta 1808: 399-404, 2011.

162. Zielenski J, Rozmahel R, Bozon D, Kerem B, Grzelczak Z, Riordan JR, Rommens J and Tsui LC: Genomic DNA sequence of the cystic fibrosis transmembrane conductance regulator (CFTR) gene. Genomics 10: 214-28, 1991.

163. Zoghbi ME and Altenberg GA: Hydrolysis at one of the two nucleotide-binding sites drives the dissociation of ATP-binding cassette nucleotide-binding domain dimers. J Biol Chem 288: 34259-65, 2013.